Open Ceramics 26 (2026) 100939

Contents lists available at ScienceDirect

Open Ceramics

journal homepage: www.sciencedirect.com/journal/open-ceramics

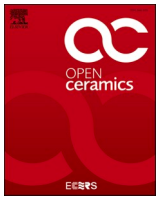

Sustainable construction materials based on mildly alkali activated waste electrical and electronic equipment (WEEE) glasses: Design and characterization

Emanuele De Rienzo [a], Francesco Carollo [b], Antonio D'Angelo [c], Luisa Barbieri [a], Enrico Bernardo [b], Michelina Catauro [c], Cristina Leonelli [a], Isabella Lancellotti [a,*]

[a] Department of Engineering "Enzo Ferrari" (DIEF), University of Modena and Reggio Emilia (UniMoRe), Via Pietro Vivarelli 10, 41125 Modena, MO, Italy
[b] Department of Industrial Engineering, University of Padova (UniPd), Via Marzolo 9, 35131 Padova, PD, Italy
[c] Department of Engineering, University of Campania "Luigi Vanvitelli" (UniCaLV), Via Roma 29, 81031 Aversa, CE, Italy

ARTICLE INFO

Keywords:
AAM
Mortar
Glass
Waste valorization
Mild activation

ABSTRACT

Glasses recovered from the ever-growing electrical and electronic equipment waste stream (WEEE) tend to be ineligible for "closed loop" recycling due to contamination from metallic, polymeric, and ceramic equipment components. They often end up in landfills unless open loop approaches are applied. As amorphous silicates, these glasses are promising candidates as recovered precursors in low-emission, low-energy production of alkali-activated materials (AAMs) for construction, with surface-focused "mild" alkali activation further enhancing process sustainability by reduced reliance on synthesized activators. Waste glass powder from fluorescent lamps and photovoltaic panels was activated and consolidated at low temperature, both on its own and in combination with sand-like fillers from volcanic rock quarry tailings. Characterization from chemical, morphological, mechanical, and antimicrobial activity standpoints showed varying degrees of success in activating the waste-derived precursors, and allowed the selection of several formulations of sustainable AAMs with desirable properties.

Abbreviations glossary

3-D: 3-dimensional
AAM: Alkali-activated material
COAR: coarse fluorescent lamp glass cullet (d = 125–2000 μm) used as filler in alkali-activated mortars
CP: closed porosity
d: diameter
EEE / WEEE: Electrical and electronic equipment / Waste electrical and electronic equipment
FLG: Fluorescent lamp glass
GR: Italian province of Grosseto
h: hour
ICP-MS: Inductively coupled plasma mass spectrometry
IHD: inhibition halo diameter
kN: kiloNewton
LAP: coarse lapillus (d = 125–2000 μm) used as filler in alkali-activated mortars
MA: State of Massachusetts, USA
ML: mass loss
MPa: megapascal
mS/m: milliSiemens per meter
Mt: Megatonne
μm: micrometer
OP: open porosity
OPC: ordinary Portland cement
Ø45: granulometry range for sieved glass precursors, defined by particle diameter under 45 μm
Ø63: granulometry range for sieved glass precursors, defined by particle diameter of 45–63 μm
Ø125: granulometry range for sieved glass precursors, defined by particle diameter of 63–125 μm
PVG: Photovoltaic glass
rpm: rounds per minute
ρ_{app}: apparent density
ρ_{geom}: geometric density
ρ_{true}: true density
SEM: Scanning electronic microscopy
σ: compressive strength
TP: total porosity
VT: Italian province of Viterbo
wt %: percentage in weight
XRD: X-ray diffraction
XRF: X-ray fluorescence

(*continued on next column*)

(*continued*)

(*continued on next page*)

* Corresponding author.
E-mail address: isabella.lancellotti@unimore.it (I. Lancellotti).

https://doi.org/10.1016/j.oceram.2026.100939
Received 9 October 2025; Received in revised form 4 February 2026; Accepted 10 March 2026
Available online 10 March 2026

(*continued*)

kV: kiloVolt	POM: coarse pumice (d = 125–2000 μm) used as filler in alkali-activated mortars

1. Introduction

When dealing with recovery of inorganic waste, glass is widely considered to be among the most recyclable materials, as its chemical stability and durability lead to a preservation of its properties over the course of several cycles of remelting and allow a 100 % recycling rate, on a theoretical basis. In practice, fully circular reintegration of glass waste into production is limited by challenges linked to its separation from externalities and sorting by composition or property affinity [1]. The conditions for an ideal "closed loop" recycling, i.e., the complete repurposing of material derived from a discarded product in the manufacturing of a second-generation product, closely replicating the makeup and function of the original with minimal mass and quality loss, often cannot be met due to the mixing of different typologies of glass waste with each other and with other types of waste materials upon collection. The wide variety of glass and glass-incorporating products leads to both cross-contamination among glasses of different composition, and contamination from metal, polymer, and ceramics externalities [2]. Such circumstances create complications during the process of remelting by which glass is remanufactured and can lead to a decrease in quality in second-generation products. In the interest of sustainability, alternative strategies of "open-loop recycling", by which glass waste is valorized as secondary raw material in the production of items that are functionally distinct from the ones of origin, are deemed necessary to boost recycling rates and to prevent excessive landfilling, which leads not only to lost value, but increased risk of contaminants within the waste glass leaching into soil and groundwater [3].

In recent years, numerous studies focused on the implementation of waste glass as a precursor in the production of alkali-activated materials (AAMs) [2–8], a class of innovative, low-impact building materials in which interest is rapidly growing, in the field of sustainable research. The fundamental mechanism at the root of alkali activation consists in the partial dissolution of a silicate powder substrate into an alkaline "activating" solution, leading to hydrolysis and recondensation of SiO_4 tetrahedral units into a polymer-adjacent cross-linked 3-D framework, embedding water from the alkali solution within itself and thus forming an amorphous gel phase. The most commonly researched and utilized subcategory of AAMs in the construction sector tend to be geopolymers, developed from aluminosilicate precursors forming zeolite-like structures out of recondensed SiO_4 and AlO_4^- units, negatively charged and balanced by counterions from the activating solution [1,9]. The amorphous structure and silicate-rich composition of multiple varieties of waste glass were proven as viable powder substrates in the development of AAMs, mostly when added a supplement to more established aluminosilicate precursors for the production of geopolymers, such as metakaolin or fly ash [3,4,10].

The main advantage linked to implementation of AAMs as an alternative to established building materials such as ordinary Portland cement (OPC) and tile ceramics, as previously anticipated, stems from the limited resource consumption and lower greenhouse gases emissions linked to their production process. The industry of cement production is among the leading sectors in fossil fuel consumption and GHG emissions, being responsible for 12–15 % of all industrial energy consumption and 5–8 % of total anthropogenic CO_2 emissions worldwide [11,12]. Considering the emissions inherently caused by both the reaction of limestone calcination itself and the fuel consumption required to trigger the reaction via temperatures up to 1000 °C, 1 Mt of CO_2 is approximately released in the atmosphere for each of the 4100 Mt of cement produced globally in a year [13]. Similarly, heavy reliance of the ceramic industry on high-temperature firing processes for production of brick and tile, along with operations of natural resources extraction and mines rehabilitation [14,15], leads to the emission of 0.256 kg CO2 for every ton of manufactured product, resulting in the release of around 400 Mt of CO2 globally in a year [16]. Such prohibitive impacts related to energy and material resource consumption can be avoided in the production of AAMs from recovered silicates, as the process does not require mining for extraction of raw materials and yields consolidated products at temperatures below 80 °C without a calcination step. Reports on implementation of metakaolin- and waste-based AAMs in place of Portland cement show that a reduction in cost up to 30 % and in emissions up to 80 % can be achieved [11].

However, one significant aspect of the alkali activation process that may be improved from a sustainability standpoint is the requirement of highly concentrated activating solutions: conventional geopolymerization typically employs sodium hydroxide (NaOH) alkaline solutions in the 8–12 M concentration range or combined NaOH–Na_2SiO_3 activators, generating pH values above 14.8 and promoting extensive dissolution of the aluminosilicate precursors [17]. Such solutions represent a more significant impact than the water utilized for activation of one-part cements due to its synthesis requirements [13] and are more dangerous to handle, leading to problems in process upscaling. Previous works [5–8,18,19], conversely, have succeeded in developing viable AAM formulations through a strategy of "mild" alkali activation, consisting in utilizing diluted alkaline solutions (2–3 M NaOH) to promote surface-level activation of the silicate precursors. The alkaline environment (pH ≈ 14.3–14.6 at 25 °C) disrupts surface Si-O-Si bonds in the glass, leaving a 'hydrated' layer of Si-OH groups, that subsequently condensate and recreate siloxane bridges among glass particles, yielding a consolidated material while foregoing the extensive dissolution and gel formation characterizing geopolymerization [5]. Compared to conventional alkali or silicate-activated AAM systems, mild alkali activation was shown to reduce alkali consumption and thus improve the environmental footprint of the products, while still enabling controlled chemical activation of glass-rich waste streams [20].

Given its advantages, the present work aims to apply mild activation as a strategy for valorization of glasses derived from waste electrical and electronic equipment (WEEE), treating them as the main precursor in the development of alkali activated matrices to be employed as base for mortars. The intent is to test the susceptibility of two distinct waste glass streams to activation via diluted alkali solution, and assess their stability and properties as building materials via a diverse array of characterization tests, in order to offer a preliminary assessment of their suitability as construction materials. The two glasses that were chosen, sourced from spent fluorescent lamps and dismantled photovoltaic panels respectively, represent interesting candidates for mild activation in particular, partially due to their intrinsically low alumina content which would limit aluminum availability for geopolymer gel formation, but would have little effect in more surface-level inter-particle bridging [21,22]. Moreover, WEEE streams in general are considered of notable interest for open-loop recycling, as they produce waste at a rapidly increasing rate due to continuous innovations in the sector, and they often incorporate a diverse mixture of materials by nature of the complex makeup of electrical and electronic products. These conditions result in rapidly growing streams of waste material that are also highly contaminated, posing unique challenges upon collection and sorting [23]. 1.5 billion units of fluorescent lamps are produced per year worldwide [24,25], and the glass from their husks are often destined to landfills [26] due to high content of mercury; an extremely toxic and persistent contaminant that determines the classification of the waste stream as hazardous even after the discarded products have undergone removal process [25], and therefore disincentives attempts at traditional recycling. Similarly, the glass that is recovered from photovoltaic panels is prone to heavy metal contamination from structural and electrical components of the device [27,28], posing a particular leaching hazard if destined to landfill [28,29]. Pursuit of innovative upcycling strategies

that might allow the safe reutilization of such waste streams is evidently compelling and represents a driving force in the experimental work here documented.

Two additional non-glassy waste streams were considered for valorization, as tailings from quarries of pumice and lapillus were employed as a coarser, mortar sand-like filler fraction in the development of alkali activated mortars. These aluminosilicates of volcanic origin were chosen due to their affinity in composition to the glass precursors, in order to promote partial reactivity and better cohesion within the activated matrix [30]. The finer fraction of both tailings ($d < 3$ mm) was chosen because of its limited marketability for other established forms of reuse for coarser fractions in horticulture or building insulation, therefore requiring storage and entailing additional costs for producers [31]. Implementation in AAM might prove effective in valorizing an otherwise undesirable fraction of discarded material.

After AAM formulations were developed, characterization tests were performed to verify the reactivity of the precursors and determine chemical stability and mechanical performance. Structural integrity over prolonged immersion in water was observed. X-ray diffraction and Fourier Transform Infrared (FT-IR) spectroscopy analyses were performed to determine the formation of new crystalline or amorphous phases within the activated matrices. Scanning electronic microscopy (SEM) was applied to observe the morphology of the materials. Compressive strength, density, and porosity of compact monolithic samples were assessed. Leaching tests were performed according to EN 12,457 European standard for hazardous waste classification in order to gauge both release of potential pollutants from the AAMs relative to health hazard threshold, and dispersion of more prevalent matrix components such as Si, Na, Al, Ca, for quantification of chemical integrity and correlation to antimicrobial properties of the materials.

Finally, the antimicrobial activity of pastes and mortars was also evaluated, as it represents both a useful metric for assessing the potential implementation of AAMs in applications such as the design of domestic surfaces [32] and an indicator of material stability. Moreover, examining antimicrobial activity against both Gram-positive and Gram-negative bacteria provides valuable insight into how these materials respond to biotic stresses from the environment.

2. Materials and methods

2.1. Materials

The fluorescent lamps glass (hereby referred to as FLG) was supplied by Treee s.r.l. (Rho, Milan, Italy) as coarse cullet, previously separated from mercury and phosphates. The photovoltaic panel glass (hereby referred to as PVG) was supplied by Garc Ambiente S.p.A. (Carpi, Modena, Italy), as coarse fragmented grains. The pumice and lapillus utilized as mortar sands were supplied by Europomice s.r.l (Milan, Italy), and mined at "Poggio Nardeci" in Pitigliano (GR), Tuscany, and at "Monte Cellere" in Cellere (VT), Latium, respectively. The composition of all materials was analyzed via X-Ray Fluorescence (ARL ADVANT'X Series, Fisher Scientific Inc., Waltham, MA, USA), and their inorganic oxides contents are reported as weight percentage in *Table 1* [33,34]. The NaOH 3 M activating solution (8.34 % Na_2O) was prepared by dissolution of laboratory-grade sodium hydroxide pellets (96 wt %, Sigma Aldrich, Italy) in distilled water.

2.2. Alkali activated pastes and mortars preparation

Both precursors underwent activation via the same procedure. After grinding in a ceramic ball mill, the WEEE glasses were sieved into distinct granulometric ranges, hereby referred to as Ø45 ($d < 45$ μm), Ø63 (45 μm $< d <$ 63 μm), and Ø125 (63 μm $< d <$ 125 μm), to be separately utilized. *Table 2* displays D10, D50, and D90 values, obtained by laser particle size analyzer (Malvern Instruments, model Hydro200S, Malvern, UK). for the utilized granulometric ranges of glass. Data confirm the nominal particle size obtained with the sieving procedure and the behavior of the two kind of glasses is very similar. Activation was carried out by suspension of the precursor in NaOH 3 M solution (2:1 solid-to-liquid mass ratio) and continuous magnetic stirring for 3 h at around 500 rpm. The activated suspensions were then transferred to silicone molds and cured in an electric oven for 72 h at a constant heat of 75 °C. The process yielded cubic monoliths that, upon demolding, were left to rest in sealed plastic bags for 24 h before characterization tests.

Mortar-like AAM formulations were prepared by incorporating fillers made up of coarser fractions of pumice, lapillus, and glass, in proportions meant to simulate the mixed grain size of mortar sand, comprising $d = 1000$–2000 μm (35 %), $d = 500$–1000 μm (34 %), and $d = 125$–500 μm (31 %). The fillers were implemented as a 20 wt % addition to glass (1:5 mass ratio) before activation and stirring, to allow exposure to the activator solution and promote surface reactivity and cohesion between fillers and matrix.

Table 1
Chemical composition wt % (XRF) of materials employed in AAMs production.

Oxide wt %	FLG	PVG	Pumice	Lapillus
SiO_2	68.47	72.02	56.60	49.10
Al_2O_3	2.26	0.86	18.60	18.30
Fe_2O_3	0.08	0.12	3.94	9.15
TiO_2	/	0.05	0.54	1.08
CaO	5.13	9.46	3.06	9.27
MgO	2.98	3.63	1.17	4.25
K_2O	1.61	0.37	8.55	3.66
Na_2O	17.65	12.00	1.98	2.35
P_2O_5	/	0.01	0.13	0.45
SO_3	/	0.29	0.13	/
Mn_3O_4	/	/	0.13	0.14
SrO	/	0.18	/	0.11
ZrO_2	/	0.06	0.07	/
CdO	/	0.03	/	/
SnO_2	/	0.02	/	/
Sb_2O_3	0.08	/	/	/
TeO_2	/	0.03	/	/
BaO	0.95	0.14	/	0.09
PbO	0.79	0.19	/	/
L.O.I	/	0.53	4.84	1.44

Table 2
Values of D10, D50 and D90 for each granulometric range of glass precursor utilized for development of viable formulations.

Glass precursor size ranges		D10 [μm]	D50 [μm]	D90 [μm]
FLG	**Ø45**	2.78	19.73	48.46
	Ø63	4.15	42.93	68.39
PVG	**Ø45**	2.36	18.08	46.28
	Ø63	4.06	43.68	68.21

2.3. Characterization

Samples for characterization were prepared in two different sizes: tests requiring either a powdered sample (XRD, ICP-MS leaching eluates analysis, antimicrobial activity) or a low-volume bulk solid sample (integrity, SEM) were carried out starting from 10 mm x 10 mm x 10 mm consolidated monoliths, while mechanical performance assessment was carried out on larger monoliths (25 mm x 25 mm x 25 mm) to gauge the cohesion of the materials in samples with a higher likelihood of crack development.

2.3.1. Chemical stability and structural integrity

An integrity and chemical stability test was performed on the obtained AAM formulations according to a procedure applied in previous studies on similar alkali activated materials [10,35,36]. Monolithic samples were submerged in distilled water (1:100 solid-to-liquid mass ratio) for 24 h and, afterwards, examined for changes in texture and

signs of dissolution in water (disintegration and loss of debris, appearance of cracks). The ionic conductivity of the eluates was measured for quantification of ions release over the submersion period, via Eutech XS Cond 6+ conductivity meter. Mass loss was assessed by measuring the mass of the samples before and after the full 24 h of submersion, 3 h of drying in acetone, and 2 h allowed for solvent evaporation. For each separate AAM formulation analyzed, values of ionic conductivity and mass loss are reported as the average of the results obtained from application of the procedure to 3 separate samples.

2.3.2. Mineralogical analysis

Precursors were screened for presence of crystalline phases before and after activation via X-ray diffraction (XRD). A PANalytical X'Pert Pro diffractometer (Malvern Panalytical Ltd., Malvern, UK) was utilized, relying on nickel-filtered Cu-Kα radiation, generated at 40 kV voltage and 40 mA current. An X'Celerator detector collected the fractions on a 2θ range of 5–90° (step size of 0.013°, 118 s scan time), and patterns were identified and correlated to a reference database of mineral phases via HighScore Plus software.

2.3.3. Microstructural analysis

FTIR spectroscopy analyses were performed to observe the presence and development of characteristic chemical bonds in the glasses before and after activation, identified by the frequency of their vibration modes. A Bruker Vertex 70 spectrometer (Bruker Ltd., Billerica, MA, USA) was employed to conduct 32-scans measurements over the 4000–600 cm^{-1} spectral region with a 2 cm^{-1} resolution, and data sets were elaborated via Bruker's Opus software.

2.3.4. Microstructural characterization

The morphology of AAM samples and precursors was examined via high-resolution scanning electronic microscopy (SEM), to determine degree of activation and evaluate interface connectivity upon inclusion of fillers. The samples were coated in metallic gold for surface electron conductivity and examined via a Nova NanoSEM 450 electronic microscopy apparatus (Thermo Fisher Scientific Inc., Waltham, MA, USA; Bruker Ltd., Billerica, MA, USA) at a 20 kV accelerating voltage.

2.3.5. Mechanical characterization (density and porosity, compressive strength)

The geometric density (ρ_{geom}) of consolidated samples was evaluated by considering the mass-to-volume ratio of cubic samples (25 mm × 25 mm × 25 mm). The mass of the samples was measured with an analytical balance and the volume with a digital caliper. The apparent (ρ_{app}) and the true density (ρ_{true}) were measured by using an Ultrapyc 3000 helium pycnometer (Anton Paar S.r.l., Rivoli, Italy), considering bulk or finely crushed samples, respectively. Average density value from five samples was used to compute the values of open (OP), closed (CP) and total porosity (TP). The compressive strength of AAMs was determined by using a Quasar 25 Universal Testing Machine (Galdabini S.p.a., Cardano al Campo, Italy) with 25 kN maximum load, following the UNI EN 826 European standard and operating with a crosshead speed of 0.5 mm/min, on cubic samples (25 mm × 25 mm × 25 mm). Formulations were tested after 28 days, which is the standard hardening period before compressive strength testing of cements and mortars. For each formulation, 5 samples per were tested and the results were averaged. Comparisons were drawn between the characterized alkali-activated systems and commercial construction materials by means of density-compressive strength charts, developed based on data stored in the latest version of the software Ansys CES (Cambridge Engineering Selector, EduPack, version 2025 R1), with new glass-based cementitious materials introduced as additional entries.

2.3.6. Standardized leaching test

Precursors and AAMs were tested following the EN 12,457 European standard for waste characterization [37], for the purpose of quantifying the release of silicon, sodium, potassium, calcium, aluminum, and various metal pollutants and micro-components in leachates, by means of inductively coupled plasma mass spectrometry (ICP-MS). In compliance with standard procedure, 5 g of sample for each formulation were ground and sieved to a particle size below 2 mm, placed within Teflon™ containers, submerged in distilled water (1:10 solid-to-liquid mass ratio), and magnetically stirred for 24 h in order to homogenize and maximize contact between liquid and ground solid. Leachates were separated from solids by filtration through sterile 0.45 μm filters, and acidified to pH = 2 with HNO_3 Suprapur® 65 wt % to avoid cation precipitation in preparation for spectrometric analysis, performed via ICP-MS iCAPTQ spectrometer (Thermo Fisher Scientific Inc., Waltham, MA, USA). The liquid samples were diluted in HNO_3 Suprapur® 2 wt % solution before the analysis, and concentrations in the original leachates were calculated taking dilution into account.

2.3.7. Antimicrobial activity analysis

The slightly modified Kirby-Bauer method has been used to examine the samples' antibacterial activity [38]. For this purpose, 200 mg discs were made by finely grinded and compressed samples. These discs were then directly exposed a one-hour UV sterilization time before their plating on Petri plates containing media and bacteria. Bacteria solutions were prepared by dissolving *Escherichia coli* ATCC25922 and *Enterecoccus faecalis* ATCC29212 pellets into NaCl 0.09 % solutions at 10^5 CFU/mL of microbial strain. The bacteria have been incubated both with and without the samples after being plated on their own agar-based solid media (TBX and Slanets-Bartley media, respectively). *E. coli* was incubated for 24 h at 44 °C, while *E. faecalis* was incubated at 36 °C for 48 h. Following microbial growth, the inhibition halo diameter (IHD, cm) was assessed. Every Petri plate has undergone four measurements and data were expressed as Mean ± Standard deviation.

3. Results and discussion

3.1. Chemical stability and structural integrity

The ionic conductivity and mass loss values provided significant information about the resistance of the inter-particle bonding formed within the AAMs after prolonged contact with water. Values of mass loss for tested formulations are reported in *Table 3* and the trend of ionic conductivity in the eluates are reported in *Fig. 1*. Activated FLG samples developed from both Ø45 and Ø63 granulometric ranges, before any addition of fillers, displayed high stability upon water immersion testing, in the form of persistent structural integrity (no development of visible surface cracks or instances of severe disintegration, marginal loss of fine debris mostly affecting the Ø63 samples), low mass loss, and low ionic conductivity of the eluates (< 30 mS/m). The formulation obtained

Table 3
Mass loss data on mortars and filler-less pastes based on FLG and PVG, obtained over the course of integrity tests.

AAM mortars			ML [%]
FLG	**Ø45**	**(no fillers)**	**6.8 ± 0.4**
		POM	6.1 ± 0.5
		LAP	6.5 ± 0.7
		COAR	4.7 ± 0.5
	Ø63	**(no fillers)**	**8.2 ± 0.6**
		POM	5.3 ± 0.4
		LAP	5.8 ± 0.6
		COAR	5.4 ± 0.6
	Ø125	**(no fillers)**	**16.1 ± 1.4**
PVG	**Ø45**	**(no fillers)**	**7.2 ± 0.6**
		POM	7.1 ± 0.9
		LAP	8.6 ± 1.0
	Ø63	**(no fillers)**	**7.9 ± 0.6**
		POM	7.7 ± 0.3
		LAP	8.5 ± 1.9

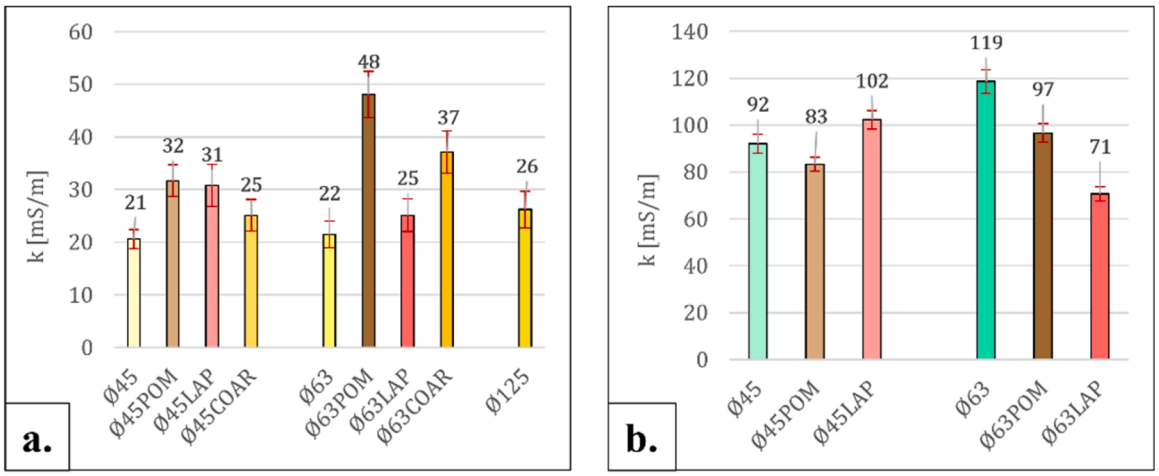

Fig. 1. Ionic conductivity measured for eluates of FLG-based AAMs (a.) and PVG-based AAMs (b.) after integrity test. [REQUIRES COLOR IN PRINT].

from activation of the Ø125 granulometric range of precursor, on the other hand, was immediately deemed unviable due to the substantial loss of mass and hardness registered after immersion, denoting the formation of an insufficiently stable activated matrix, and was discarded in further experimentation. Beyond the extreme instance represented by the Ø125, a finer grain size range was slightly favored from an ion dispersion and mass loss point of view when comparing the performance of Ø45 and Ø63 pastes, a difference that can be ascribed to the more extensive available surface that the finer precursor provides for the alkali-induced formation of siloxane bridges. Previous studies on applications of waste glass in concrete and AAM formulations have highlighted correlation between finer particle size and enhanced pozzolanic activity and matrix cohesion [39-41]. Activated PVG does not distinguish itself significantly from FLG in terms of mass loss trends, although PVG immersion eluates present a markedly higher conductivity, up to 120 mS/m. Such a discrepancy in ion dispersion between two activated glasses could be a consequence of different degrees of activation, as the hydroxide solution employed to activate PVG might have promoted inter-particle condensation to a lower extent and remained inactive within the structure, forming separate phases that dissolve upon immersion in water and release unreacted hydroxide ions that cause an increase in eluate conductivity [30].

Addition of fillers to FLG paste led to development of hardened monoliths that were less subject to mass loss upon immersion compared to their non-reinforced counterparts, while presenting slightly higher ion release in their eluates (*Fig. 1a*), attributable to the higher concentration of metals prone to dissolution as trivalent ions (Al, Fe) within pumice and lapillus. It is worth noting that coarse FLG cullet also had the effect of raising ion release when added as filler, possibly by virtue of the lower reactivity of the filler particles compared to the finer precursor ones leading to an overabundance of unreacted hydroxide within the structure. The PVG matrix appears to be differently influenced by addition of fillers, compared to FLG: while eluates conductivity appears to decrease with the presence of pumice and lapillus in the system, values of mass loss are reportedly higher for monoliths incorporating lapillus, and essentially comparable to non-reinforced PVG samples for ones incorporating pumice (*Fig. 1b*). This suggests a generally more extensive activation in filler-added PVG formulation compared to ones obtained from PVG, given the lower ion dispersion, and the formation of a more soluble activated phase in the case of lapillus addition.

3.2. Mineralogical analysis

XRD analysis yielded predominantly amorphous diffractograms for all analyzed formulations, in close proximity to the signal of the non-activated glass precursors (*Fig. 2*). Traces of similar crystalline phases

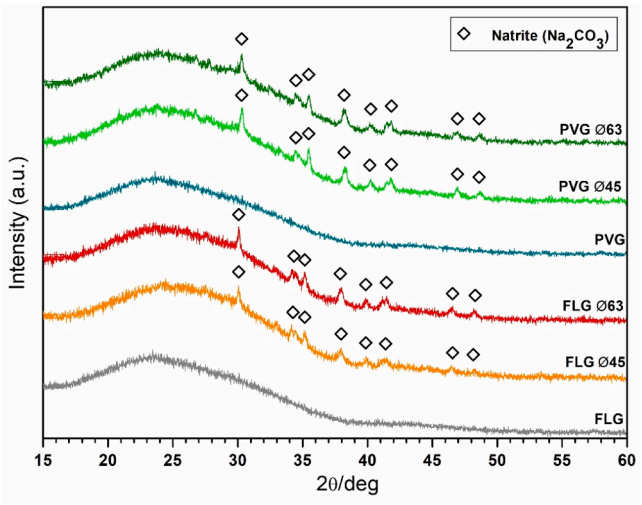

Fig. 2. XRD patterns of FLG and PVG glass precursors and AAMs, distinct by granulometry. [REQUIRES COLOR IN PRINT].

were detected across formulations and identified as sodium carbonate (Na_2CO_3, natrite), a species that is frequently observed to be forming as a side effect of alkali activation on the surface of silicates; when the slurry presents surplus of unreacted hydroxide ions from the activating solution, such ions react with atmospheric carbon dioxide to form carbonate as surface efflorescence during consolidation of the AAMs [42]. No apparent shifts in the amorphous signals (broad band at $2\theta^\circ = 18–38$) towards higher or lower diffraction angles are detected across analyzed AAMs compared to their precursor, which might be reflective of the superficial nature of the activation of glass particles, not leading to any deep or extensive alteration of the original amorphous structure of the glass. Similar intensities are reported for the natrite peaks of maximum height in the diffraction patterns of all samples, hovering in the 500–600 counts range, suggesting analogous development of carbonate across formulations. Very slight differences in development of carbonates were observed between samples of different grain size in both glasses, via Calcimeter (Dietrich-Frühling) measurements: a lower amount of carbonates was reported for Ø45 samples (5.5 % for PVG and 7 % for FLG, compared to 6.6 % and 10 % for Ø63 samples of PVG and FLG respectively), confirming more thorough activation of precursors of finer grain size.

3.3. Microstructural analysis (FT-IR spectroscopy)

FTIR spectroscopy corroborated the formation of carbonates in the glass upon alkali activation, already signaled by the diffractograms. Peaks associated with vibrations of the C—O bond previously absent from the non-activated glass, namely in the 1420–1430 cm^{-1} and the 860–880 cm^{-1} range [43,44], appear on the spectral profiles for all activated formulations (*Fig. 3*). The behavior of the main 960–970 cm^{-1} peak across samples, associated with asymmetrical stretching of the Si-O-Si bond [45] is another salient aspect of the spectral profiles. Rather than undergoing a shift towards higher wavenumbers commonly observed in alkali-activated aluminosilicates [44,45], corresponding Si-O-Si peaks between AAMs and their respective starting glass display close overlap in frequency, suggesting that the activation of the glass did not determine a deep alteration of its structure or reorganization of its bonds. Such interpretation would also align with the lack of a shift in the amorphous signal from the diffractograms, reflecting the persistence of the molecular structure of the original glass and a surface-level susceptibility to activation.

3.4. Morphological characterization

SEM morphological analysis was instrumental in observing the responsiveness of the glass to mild activation, along with verifying certain hypotheses that emerged during chemical stability testing, concerning the relative degree of responsiveness of the glasses to the activator and its correlation to parameters such as precursor composition and granulometry.

FLG formulations distinct by finer and coarser matrix reported remarkable differences in morphology. The FLG Ø45 sample appears as generally homogeneous, with crystals of varied shape less than 1 μm in length dispersed on the surface and microcracks up to 8 μm-wide. Glass fragments such as the ones visible in *Fig. 4a* can be identified, but there seems to be continuous melding among single fragments, consistent with siloxane bridges formation among glass particles (*Fig. 4b*). The morphology in Ø63 samples appears instead fragmented and heterogeneous, disseminated with crystallites ascribed to efflorescing carbonates, and bigger, unreacted glass granules can be identified (*Fig. 4c*).

The most salient difference between FLG- and PVG-based pastes can be found in the development of siloxane bridges upon glass activation. Upon comparison with images of non-activated PVG (*Fig. 5a*), the Ø45 matrix morphology of activated PVG appears to have undergone partial activation when examining it at higher magnifications (*Fig. 5b*), presenting itself, however, as considerably less homogeneous than its FLG counterpart on a larger scale. The Ø63 presents an even more disjointed surface, interspersed with pronounced needle-like carbonate crystals up to 30 μm in length, and appears as less compact than its FLG counterpart (*Fig. 5c*).

The drastic difference in reactivity to alkali activation between the two glasses can be linked to their chemical composition. As previously reported in works experimenting with reactivity of glass in alkaline environment, alkaline earth elements (CaO, MgO) act as network stabilizers, which means that their presence in high percentage within the composition of a glass such as PVG determine a stronger structure and a lower tendency to solubilization; on the other hand, alkaline oxides (Na_2O, K_2O) are considered network modifiers, as they yield ions with a larger radius that disrupt the glass network in their points of insertion, meaning that their higher presence in the composition of a glass such as FLG affords higher reactivity [46]. Thus, the precursor has a more pronounced tendency to maintain its original form in PVG formulations, undergoing only partial superficial binding, while FLG formulations show a more marked solubilization and homogenization among single particles.

FLG-based mortars present a variety of distinct morphologies from their filler-less counterparts, with varying degrees of implementation of the coarser filler particles. FLG Ø63LAP is distinguished by its generally disjointed microstructure already observed in the Ø63 matrix (*Fig. 4c*), albeit with an apparently higher degree of overlap and smoother interfaces between particles, which make it resemble the more homogeneous surface structure of a Ø45 matrix, complete with microcracks under 2 μm in width (*Fig. 6*); this is possibly a consequence of the partial reactivity of the lapillus filler coming into play, contributing to interparticle bridging reactions in the glass via dissolved aluminate and silicate units and giving the activated portions of the sample a distinct morphology, also influenced by the underlying porous filler particles (wide pore size distribution, between 2 μm and 20 μm in diameter). FLG Ø63POM presents a partially homogeneous morphology comparable to its lapillus-integrated counterpart (*Fig. 7*), albeit less extensive and characterized by a higher proliferation of carbonate crystallites. FLG Ø45POM (*Fig. 8*), while displaying a more homogenized morphology compared to Ø63POM, is revealed to develop intense surface cracking (crack width up to 3 μm), along with significant crystallite proliferation.

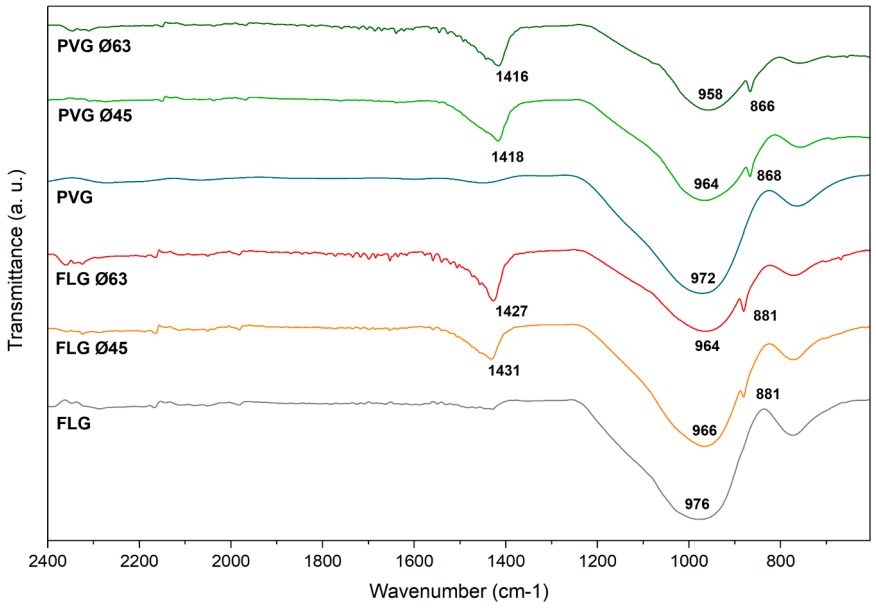

Fig. 3. FT-IR spectroscopic profiles of FLG and PVG glass precursors and AAMs, distinct by granulometry. [REQUIRES COLOR IN PRINT].

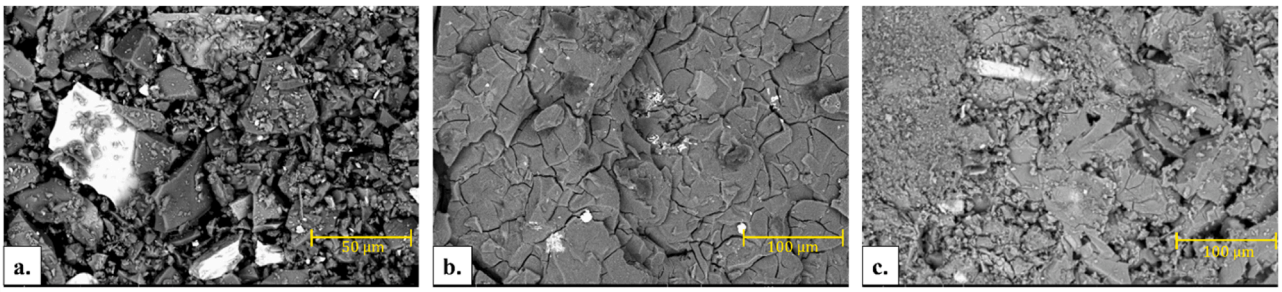

Fig. 4. SEM imaging of unactivated FLG precursor at 2000x magnification (a.), FLG Ø45 at 1000x (b.), and FLG Ø63 at 1000x (c.).

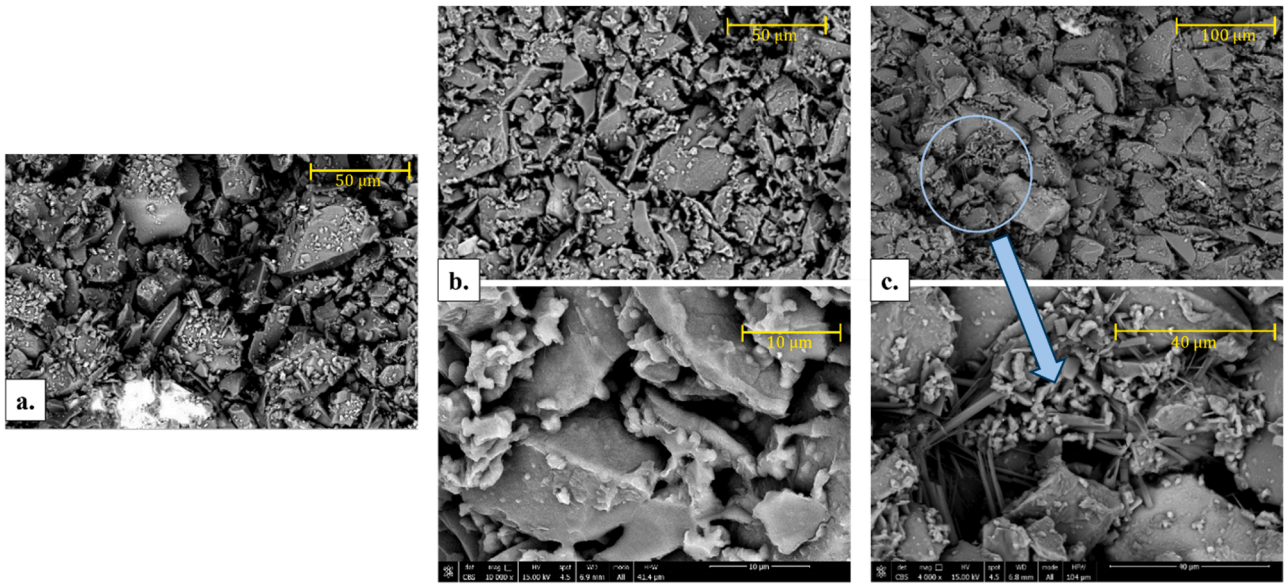

Fig. 5. SEM imaging of unactivated PVG precursor at 2000x magnification (a.), PVG Ø45 at 2000x with focus at 4000x on activated surface layer (b.), and PVG Ø63 at 1000x with focus at 4000x on carbonate crystal (c.).

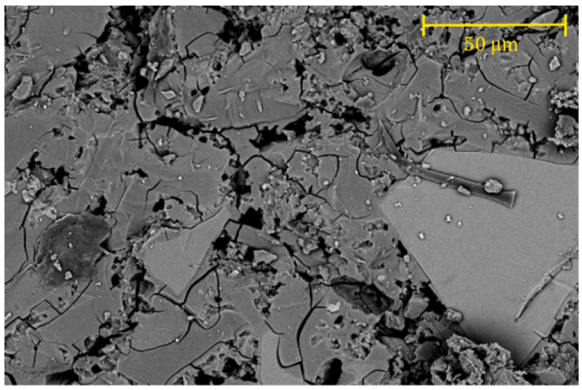

Fig. 6. SEM imaging of FLG Ø63LAP at 2000x magnification.

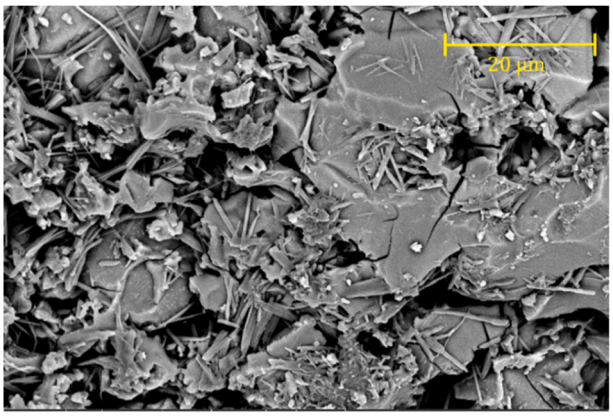

Fig. 7. SEM imaging of FLG Ø63POM at 5000x magnification.

FLG Ø45COAR, given its fully glassy composition, shares the closest similarities to non-integrated FLG matrices, as it presents a homogeneous morphology where the melding of glass particles is occasionally interrupted by coarser glass grains and agglomerates of smaller crystallites (*Fig. 9*); cracks in the homogeneous surface appear as thin (maximum width of 0.5 µm), extended, and interconnected.

The morphology of a selection of samples among PVG-based mortars possibly signal an improvement in precursor reactivity upon implementation of partially reactive fillers in a glassy matrix of lower reactivity. PVG Ø45LAP presents as more compact and homogeneous than non-integrated Ø45 paste, displays multiple instances of smooth interface between glass grains (*Fig. 10*), and is distinguished by a surface microstructure that appears closer in shape to the one formed on FLG Ø63LAP, again signaling a possible participation of the lapillus fillers to the activation reaction. PVG Ø63POM, on the other hand, appears closer in morphology to the Ø63 matrix, presenting as clusters of large, disjointed silicate particles that only appear to participate in inter-

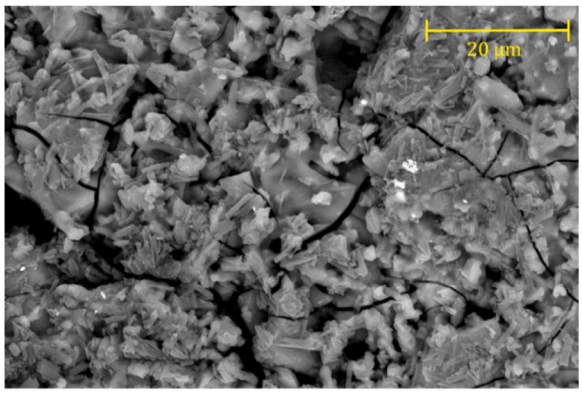

Fig. 8. SEM imaging of FLG Ø45POM at 5000x magnification.

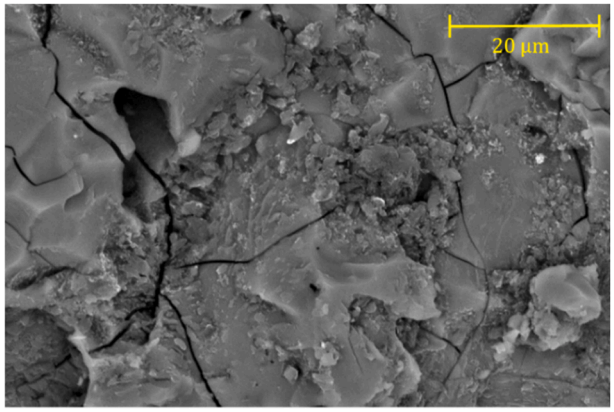

Fig. 9. SEM imaging of FLG Ø45COAR at 1000x (a.) and 5000x (b.) magnification.

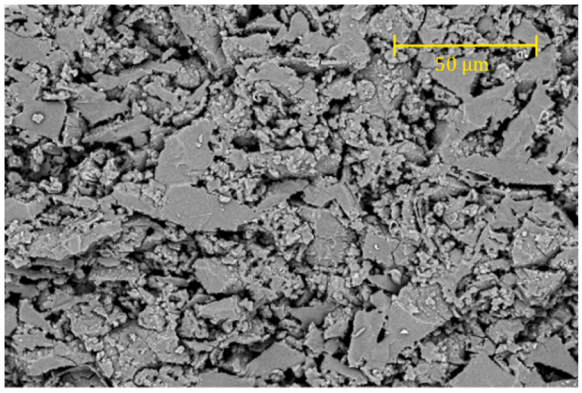

Fig. 10. SEM imaging of PVG Ø45LAP at 2000x magnification.

particle bridging with the smaller granules distributed on their surface (*Fig. 11*).

3.5. Mechanical and physical characterization

The results of mechanical tests and porosity and density measurements are reported in *Table 4*. These data sets provide insight into the mechanical performance of FLG-based and PVG-based activated pastes and mortars, revealing that the grain size distribution of the fine matrices critically influenced both the absolute values of compressive strength and the consistency of measurements across samples of the same formulations. *Table 4* also provides benchmark values of

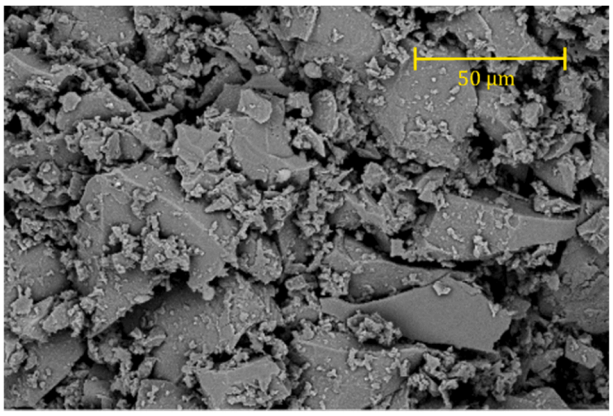

Fig. 11. SEM imaging of PVG Ø63POM at 2000x magnification.

Table 4
Density, porosity (open OP, closed CP, total TP) and compressive strength values of AAMs from FLG and PVG waste; comparison with properties of OPC mortars and AAMs based on blast furnace slag, fly ash, a 50–50 mixture of metakaolin and glass from construction waste (CW), and 100 % fiberglass.

			ρ_{geom} [g/cm^3]	OP [%]	CP [%]	TP [%]	σ [MPa]
FLG	**Ø45**	**(no fillers)**	1.95 ± 0.04	12.77 ± 1.97	2.15 ± 0.05	14.92 ± 1.92	25.24 ± 3.87
		POM	1.66 ± 0.10	31.03 ± 4.30	0.52 ± 0.03	31.54 ± 4.27	12.20 ± 2.09
		LAP	1.75 ± 0.07	28.64 ± 3.06	0.14 ± 0.01	28.78 ± 3.05	24.87 ± 7.03
		COAR	1.85 ± 0.06	20.73 ± 2.54	3.26 ± 0.10	23.99 ± 2.44	28.85 ± 5.89
	Ø63	**(no fillers)**	1.94 ± 0.03	15.60 ± 1.44	4.54 ± 0.08	20.15 ± 1.36	31.55 ± 3.00
		POM	1.66 ± 0.06	32.31 ± 2.42	0.96 ± 0.03	33.27 ± 2.39	34.06 ± 3.48
		LAP	1.66 ± 0.04	33.20 ± 1.66	0.85 ± 0.02	34.05 ± 1.64	38.76 ± 3.41
		COAR	1.81 ± 0.07	26.17 ± 2.93	0.29 ± 0.01	26.47 ± 2.92	26.84 ± 4.92
PVG	**Ø45**	**(no fillers)**	1.58 ± 0.06	34.19 ± 2.33	1.10 ± 0.04	35.29 ± 2.29	9.44 ± 4.67
		POM	1.77 ± 0.03	28.67 ± 1.29	4.50 ± 0.08	33.17 ± 1.21	20.40 ± 3.75
		LAP	1.76 ± 0.03	30.37 ± 1.38	2.55 ± 0.05	32.92 ± 1.33	29.10 ± 6.63
	Ø63	**(no fillers)**	1.70 ± 0.03	29.97 ± 1.13	0.66 ± 0.01	30.63 ± 1.12	11.68 ± 3.67
		POM	1.70 ± 0.04	32.57 ± 1.75	4.01 ± 0.10	36.59 ± 1.64	20.88 ± 1.06
		LAP	1.64 ± 0.02	35.61 ± 0.84	2.53 ± 0.03	38.14 ± 0.81	20.98 ± 6.48
OPC			1.9–2.2	/	/	20–35	40–65
Slag			2.1 ± 0.1	/	/	16 ± 1	15 ± 1
Fly ash			2.2 ± 0.1	/	/	12 ± 1	60 ± 1
MK-CW glass 50–50			2.5 ± 0.3	/	/	17.0 ± 0.1	16 ± 1
Fiberglass			1.7 ± 0.1	/	/	36.5 ± 0.1	16 ± 2

mechanical properties sourced from literature, for OPC mortars [47,48] and AAMs derived from precursors such as slag [49], fly ash [50], and other streams of waste glass [43,7] via comparable curing regime and more aggressive activation with respect to the AAMs developed in the work.

Among FLG-based mortars, those prepared using glass particles in the Ø63 grain size range exhibited better mechanical properties. These formulations consistently show compressive strength values, exceeding

30 MPa and even approaching 40 MPa across multiple replicates when enhanced with pumice or lapillus fillers. This trend highlights not only the mechanical resistance but also the reproducibility of results for this matrix type, making Ø63-based systems promising candidates for structural applications. The Ø45 matrix, on the other hand, whether integrated or not, yielded materials of poorer mechanical properties and a wider berth of compressive strength values for each formulation, with only the coarse cullet-based mortar approaching, while not consistently surpassing, the 30 MPa threshold. These samples exhibited both lower average compressive strength and greater variability between trials. The only exception was the mortar formulated with coarse cullet as filler, which approached, but failed to consistently exceed, the 30 MPa threshold. The inferior performance of Ø45-based paste and mortars could be attributed to a higher propensity for development of interconnected microcracks, displayed in the SEM morphological profiles (*Fig. 4b*, *Fig. 7*, *Fig. 8*), possibly due to the finer granulometry exacerbating sintering phenomena between glass particles during the consolidation phase [51]. An interesting pattern characterizing FLG systems thus emerges: there is not a strict correlation between chemical stability and mechanical performance, as the precursor particle size range determining better integrity of the matrix when undergoing environmental stress tends to lack in strength compared to the coarser range. This might be an argument towards the combined utilization of both granulometries in development of FLG-based AAMs, which might prove more advantageous in the context of large-scale productions, as it implies a less demanding process of grinding and sieving.

PVG-based mortars exhibited a different behavior profile with respect to ones based on FLG. The distinction between different grain sizes was less pronounced in this series, with a more uniform performance observed across Ø45 and Ø63 matrices. Furthermore, while addition of fillers to FLG matrices did not consistently determine an increase in compressive strength, all PVG-based formulations integrated with coarse pumice or lapillus reported an improvement in mechanical properties. However, such improvement was marginal, as the best performing PVG-based system proved weaker than the best performing system developed from FLG matrices. As with FLG, the highest strength values for PVG mortars were achieved through the incorporation of lapillus, with Ø45-based samples averaging around 30 MPa. It is possible that the combined effect of the coarser filler particles limiting crack formation and the partial reactivity of the lapillus itself, releasing aluminosilicate particles in the activation slurry and contributing to the proliferation of an amorphous phase that appears severely limited in the filler-less PVG Ø45 samples, promote the formation of a more cohesive structure within the Ø45 powder phase, which is already pre-disposed to higher reactivity by virtue of its finer granulometry, leading to compact monoliths that can better withstand more intense compression. However, this performance remained limited in scope and reproducibility. The relatively lower mechanical strength and higher open porosity observed in PVG-based mortars are likely to be a consequence of incomplete activation, leading to the formation of a fragmented, loosely bonded matrix that is more susceptible to mechanical failure. These findings underscore the importance of both precursor chemistry and granulometry in determining the final performance characteristics of alkali-activated systems.

A visual representation of the results obtained is provided by *Fig. 12* (FLG) and *Fig. 13* (PVG). Materials with the highest porosity content typically exhibit the lowest strength values (and highest values of 1/compressive strength) and vice versa [6]. AAMs developed from WEEE glasses are undoubtedly promising since they exhibit properties comparable to those of lightweight concretes, thanks to the combination of relatively high compressive strength and lower density mainly afforded by the inclusion of volcanic fillers and their inherently high porosity percentage. As observed from *Table 4*, the FLG Ø63 series, which encompasses the best-performing formulations, reach the lower compressive strength threshold for comparison with OPC mortar. While none of the formulations match the strength-density balance of higher-performance fly ash AAMs, the FLG pastes and the majority of FLG and PVG mortars surpass the performance of an average slag AAM, and especially of both glass-incorporating samples displayed in the table, derived from a 50–50 mixture of metakaolin and glass from construction waste, and pure fiberglass waste respectively. This can be seen as a testament to the viability of FLG as a reactive precursor in mild alkali activation, as well as the effectiveness of pumice and lapillus especially as fillers.

3.6. Standardized leaching test

Leaching tests allowed quantification of released constituent elements of the AAMs (Si, Al, Na, K, Ca), along with heavy metals and minor components. By testing both the glasses as raw material and as activated monoliths, it was determined that activation led to increased release of all identified species in the leachates, attributed to the

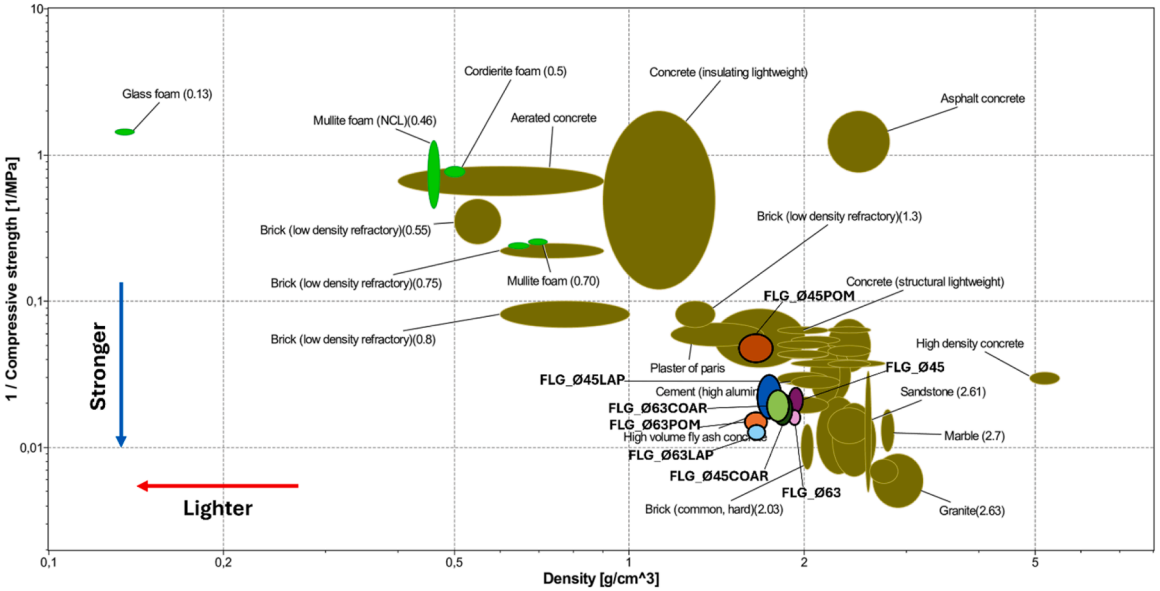

Fig. 12. Compressive strength/density trade off chart of FLG products. [REQUIRES COLOR IN PRINT].

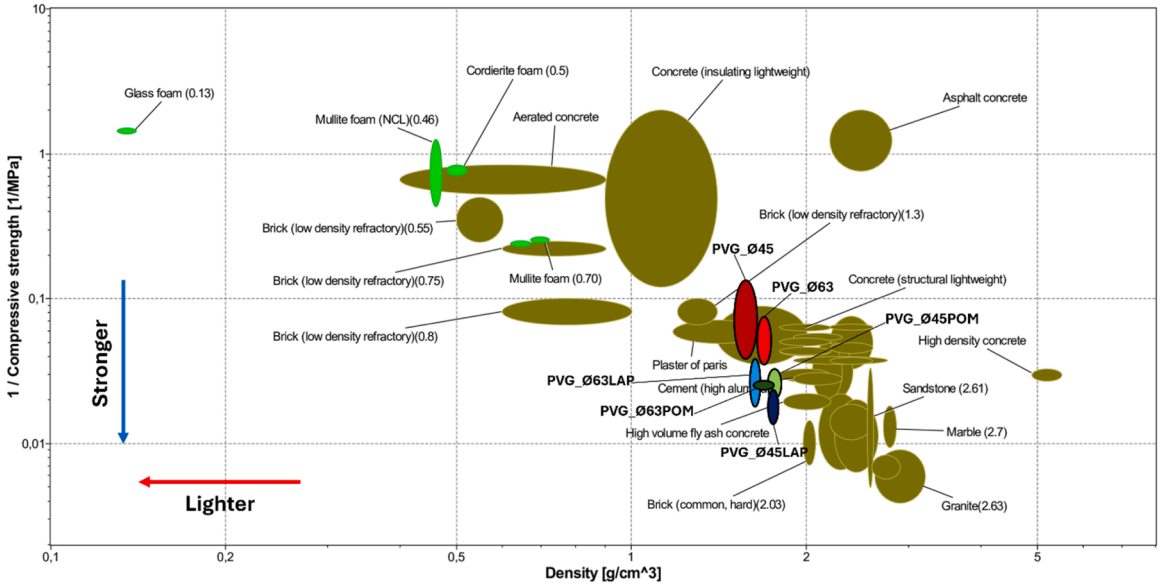

Fig. 13. Compressive strength/density trade off chart of PVG products. [REQUIRES COLOR IN PRINT].

mobilization of ions upon alkaline attack of the precursors. The different grain size in the matrices was shown to only slightly influence the

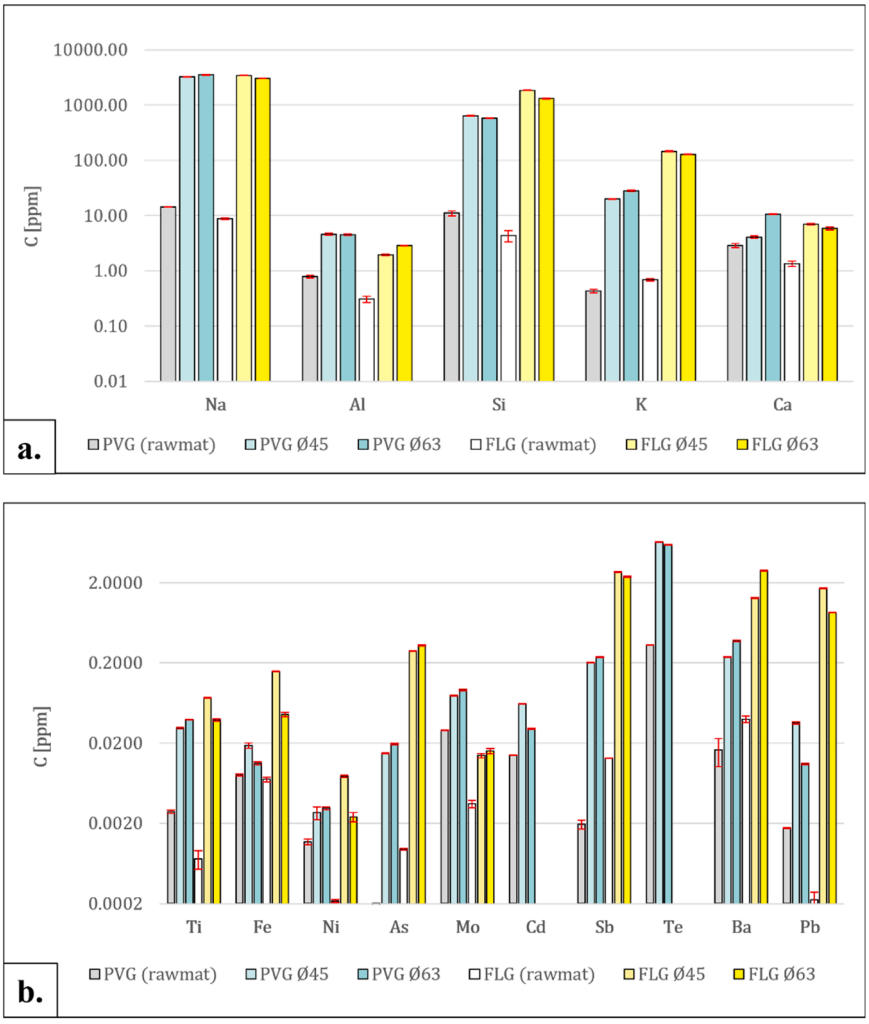

Fig. 14. ICP-MS-derived concentrations of constituent elements (a.) and micro-components (b.) in leachates from non-activated FLG and PVG precursors, and alkali-activated pastes based on FLG and PVG. [REQUIRES COLOR IN PRINT].

release values. The leachates concentrations were reported for the constituent elements in general as very low, but the difference in Si release in the two glasses confirms the more stable and less reactive nature of PVG.

With regards to FLG- and PVG-based pastes, results of quantification of constituent elements and micro-components are reported in *Fig. 14a* and *Fig. 14b*, respectively. Sodium was the predominantly released element (3162 ppm peak among mortars, beyond 3000 ppm among matrices), both present in high concentration in the glass precursors (18 % Na_2O for FLG, 12 % for PVG) and deposited from the activating solution as carbonate. Aluminum, relatively low in concentration in both precursors, displayed a slightly higher release in PVG formulations despite less significant presence in the precursor (0.86 % vs 2.26 % for FLG), possibly ascribed to more extensive activation leading to more significant structural incorporation of AlO_4^- units. Minor components quantification shows that, except for Mo (higher releases before and after activation) and Cd contained in coating present only in PVG, higher releases were mostly reported for FLG-based materials, possibly due to the glass's more pronounced susceptibility to alkali attack. Effects of activation are especially noticeable for release of amphoteric species such As and Sb, converted to a highly soluble form in alkaline environment. Cd and Te, detected exclusively in PVG, derive from traces of cadmium telluride photoactive film in the dismantled panels [52]. No overall trend linked to matrix grain size can be observed between PVG formulations, while slightly lower releases are more consistently reported for FLG Ø63 compared to FLG Ø45.

Constituents and micro-components release values for FLG-based mortars are reported in *Fig. 15a* and *Fig. 15b*, respectively. While little difference in susceptibility to release was displayed between Ø45 and Ø63 in the case of simple pastes, more definite and distinct trends linked to matrix grain size are highlighted by analysis of mortar leachates. For Ø63 matrices, the mortar incorporating coarse FLG cullet as filler (COAR) was shown to release more constituents, possibly due to the high susceptibility of FLG to solubilization determining its selective alkaline attack with respect to the volcanic fillers, that only react partially when implemented. This is particularly evident with aluminum leaching, with an especially pronounced gap between POM or LAP formulations and COAR ones, in terms of concentration released. The mere presence of less reactive particles within the matrices might also determine the lower release of constituents when compared to filler-less matrices, as the content of the volcanic fillers mostly remains unreacted in the core of the coarser particles, and the percentage of the precursor, more susceptible to leaching, is diminished by their presence. A similar trend to the one registered for macro-components can be observed for release of micro-pollutants, with pumice- and lapillus-integrated formulations presenting more contained releases compared to both the simple paste

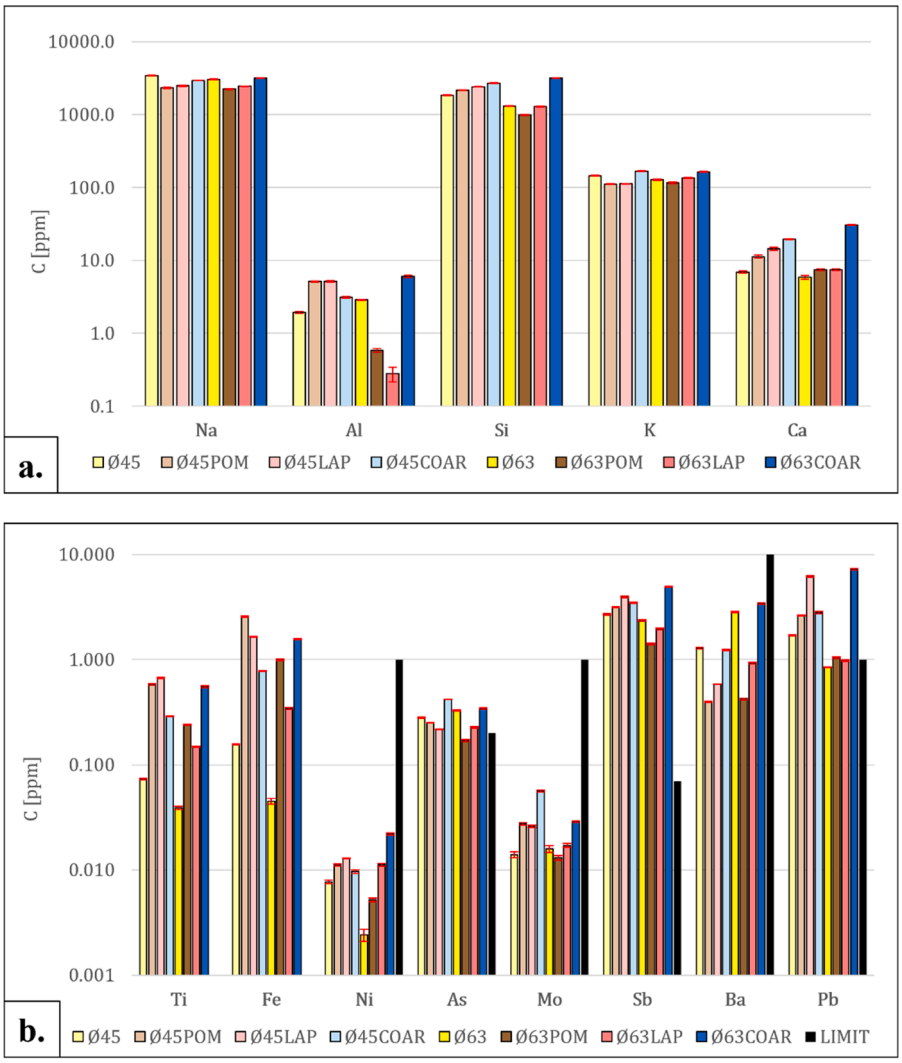

Fig. 15. ICP-MS-derived concentrations of constituent elements (a.) and micro-components (b.) in leachates from non-activated FLG precursor, and alkali-activated mortars based on FLG. Black bar signals leachate concentration limit for disposal as non-hazardous waste according to Italian Ministerial Decree 27 Sett 2010. [REQUIRES COLOR IN PRINT].

and the cullet-integrated mortar. Ø45 matrices, on the other hand, generally experienced an increase in releases of both major and minor components upon addition of fillers, relative to values reported for simple pastes. These results correlate to the worse mechanical performance of such filler-incorporating matrices compared to ones based on precursor sieved in the Ø63 range, and suggest the formation of an overall less cohesive activated matrix, less capable of withstanding both high compressive strength and prolonged environmental stress. Values for Fe and Ti release present a notable exception to these trends, being reported as significantly higher in both Ø45 and Ø63 matrices after pumice or lapillus addition due to their more pronounced presence in the volcanic aluminosilicates.

According to the constituents and micro-components releases reported in *Fig. 16a* and *Fig. 16b* respectively, addition of fillers appeared not to consistently determine lower leachates concentrations for PVG matrices, as opposed to FLG ones. Most noticeably, analysis of leachates from the mortar samples highlighted a higher Fe and Ti concentration, attributable to the substantial natural presence of the elements within the volcanic fillers, and a substantially mitigated release of Te, exclusive to the composition of the precursor. The varied dynamics of release for each element might be a signal of the further extent of activation which the volcanic aluminosilicates undergo when introduced in the same environment as a glass precursor such as PVG, less prone to dissolution and activation compared to FLG, and the differentiated partition of ions between the inert bulk of silicate grains and the activated surface. Release of more concentrated components is reported as more substantial in mortars compared to pastes. Al is an exception, which could be linked to implementation of AlO_4^- units in a more structural capacity.

Leachate concentration values obtained across all analyzed formulations for those microcomponents that are considered environmental pollutants, were compared to legislated threshold values for classification of waste as non-hazardous, established by Italian Ministerial Degree 27 Sett 2010 and referring to EN 12,457 standardized test. Threshold values are displayed in *Fig. 15b* and *Fig. 16b* for all elements of interest. FLG-based formulations present more potentially hazardous releases, with As levels slightly exceeding threshold and Sb and Pb more significantly surpassing it, while PVG-based formulations only present an excess in Sb. The presence of such ions in the original glass precursors, acting as stabilizers and refining additives within the glass reticule [53,54], and their release in the reported amounts over the 24-hour leaching test, signal both a potential hazard inherent to discarding artifacts produced out of the examined alkali-activated materials in landfills, but also the occurring of activation on the glass surface particles. This behaviour renders further optimization necessary for the activated formulations to be environmentally acceptable for real-life applications. Such an optimization could be achieved via addition of more reactive aluminosilicates precursors such as metakaolin or slag [55,56], phosphate binders and other addictives for chelation or reduction [57-59], or by carrying out carbonate curing [56,60] or simply raising the consolidation temperature, to foster a more extensive condensation of Si-OH

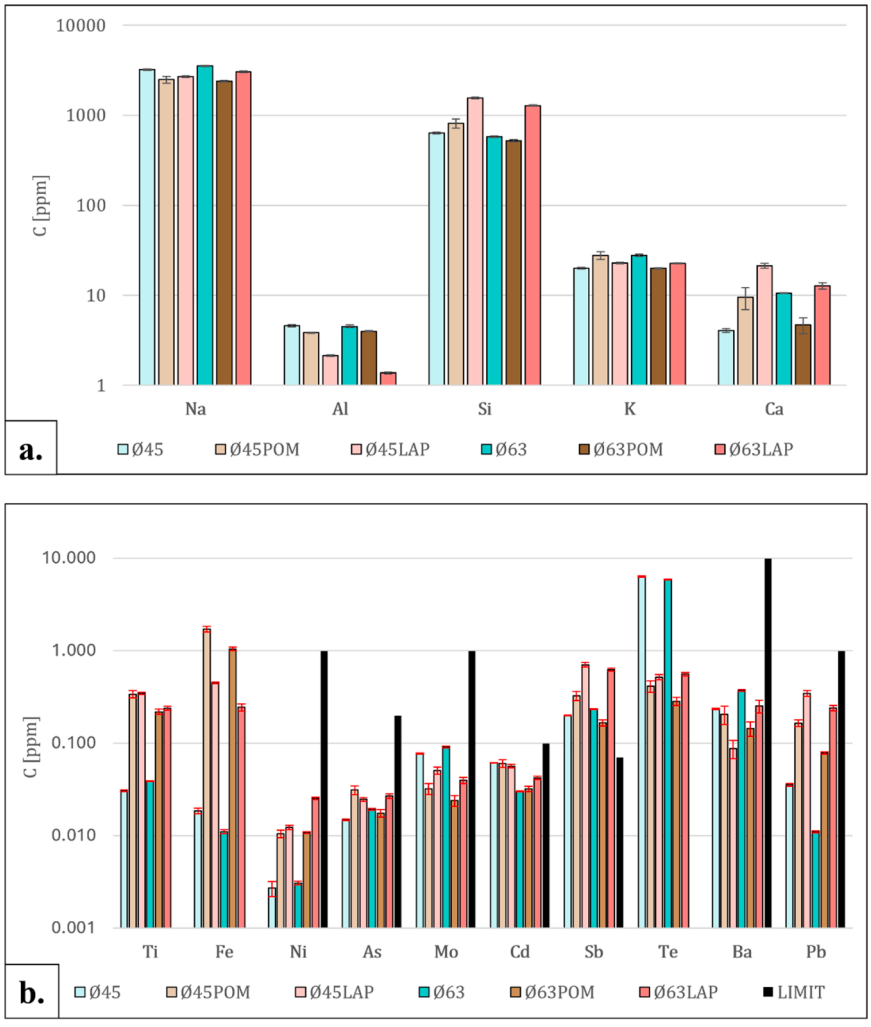

Fig. 16. ICP-MS-derived concentrations of constituent elements (a.) and micro-components (b.) in leachates from alkali-activated mortars based on PVG. Black bar signals leachate concentration limit for disposal as non-hazardous waste according to Italian Ministerial Decree 27 Sett 2010. [REQUIRES COLOR IN PRINT].

unit and proliferation of siloxane bridges among alkali-activated glass particles.

3.7. Antimicrobial activity analysis

The evaluation of the antimicrobial properties of the FLG and PVG mortars has been reported in terms of inhibition halo diameter (IHDs) obtained after incubation time of the samples with *E. coli* and *E. faecalis* strains. Regardless of the matrix particle size and the presence of pumice, lapillus, or cullet as fillers, FLG mortars showed the same antimicrobial properties (*Fig. 17a*), with respect to *E. coli* (IHD ranges from 2.5 to 2.7 cm) and to*E. faecalis* (IHD ranges from 1.3 to 1.5 cm). According to the leaching results, these trends can be explained by the combination of Na, K and Ca as macro components and, even at lower concentration, by trace elements such as Pb. Indeed, the outer membranes of both Gram-positive and Gram-negative bacteria are rich in negatively charged lipids that face the extracellular environment [61]. Calcium ions can bind to the phosphate groups of phospholipids, thereby reducing electrostatic repulsion between the polar heads. This interaction alters membrane stability and fluidity, potentially causing leakage of cellular contents and resulting in cell death [62]. Pb^{2+} may compete with Ca^{2+} bindings of phosphate groups of phospholipids and take part in metabolism resulting in cell growth inhibition [63]. Moreover, potassium ions also play a critical role in bacterial viability. Bacteria tightly regulate intracellular potassium levels to maintain osmotic balance and membrane potential. Elevated extracellular potassium can disrupt this balance by drawing water into cells through osmotic mechanisms, leading to cell swelling and mitochondrial dysfunction [64]. Additionally, potassium is essential for enzymatic and metabolic functions; its dysregulation can impair protein synthesis and other vital processes, ultimately leading to cell death [65]. Beside Ca and K ions, even the huge amount of sodium released contributes to the hyperosmotic condition that causes cell death. The increased antimicrobial activity of FLG mortars against *E. coli* strain is also enhanced by the alkaline environment (range of pH among samples was 9–10). This Gram-negative bacterium has a lower tolerance than *E. faecalis* (Gram-positive strain), which showed the lower values of IHD [66,67]. Finally, the presence of Sb does not affect the microbial growth of *E. coli* since this bacterium is able to reduce Sb(V) to Sb(III) in the extracellular matrix avoiding its toxicity [68].

Regarding PVG mortars, a different behavior can be observed according to the size and the choice of filler. Firstly, from the histogram in *Fig. 17b*, it can be seen that PVG mortars showed higher antimicrobial properties than FLG mortars (all IHD values above 2.7 cm). In particular, PVG ∅45 and ∅63 had IHD values of 4.5 and 4.2 cm that indicate a very strong antimicrobial activity since most of the bacteria could not grow. This strong enhancement can be attributable to a combination of: i) Na, K and Ca release, ii) the alkaline environment (pH between 9 and 10), and iii) the antimicrobial effect of tellurium. This latter is known as antimicrobial toxic metal since it causes prokaryotic membrane damage thus leading to cell disruptions especially with respect to gram-negative strains [69]. PVG mortars containing pumice or lapillus showed lower antimicrobial activity with respect to the PVG mortars without filler. The slightly higher antimicrobial activity of PVG ∅45 and ∅63LAP is attributable to the higher presence of leached Ca ions in microbial media. PVG ∅45 mortar showed even higher antimicrobial activity against *E. faecalis* (IHD = 2.6 cm). This behavior could be related to improved interaction between the microbial strain and the activated mortar, thus leading to higher antimicrobial activity originating from the K, Na, Ca and Te ions.

4. Conclusion

The study explored mild alkali activation as a strategy of valorization of glass from the WEEE stream, with compelling results varying on the basis of preparation parameters, glass types, and choice of Nsupplementary materials. Through characterization, specific formulations were selected that demonstrated remarkable chemical stability, along with mechanical properties comparable to those of OPC-based mortars and lightweight concretes. Mineralogical and microstructural analyses showed that mild activation did not substantially alter the structure of the starting glasses, which largely retained their amorphous nature. This suggests that the inter-particle bonding mechanism leading to AAM formation was confined to the surface of the glass grains. Throughout chemical integrity testing and morphological analysis, fluorescent lamp glass appeared drastically more susceptible to activation compared to photovoltaic glass, displaying more extensive inter-particle condensation and a more homogeneous morphology. The lower amount of stabilizer ions in its composition was considered a likely cause of such distinction in behavior.

When considering the activated pastes before filling, differences in properties linked to precursor granulometry (∅45 or ∅63) over integrity, compressive strength, leaching, and antimicrobial activity tests showed marginally better viability of a coarser precursor. Such differences were substantially amplified in FLG formulations by addition of coarse fillers, especially with regards to mechanical properties and components release in water, as mortars obtained by addition of pumice and lapillus especially to ∅63 matrices displayed a compressive strength-to-density ratio comparable to that of lightweight concretes and markedly improved ions retention, when compared to their ∅45 counterparts. This was attributed to the interaction between ∅63-sized glassy precursor and volcanic aluminosilicates in the alkaline environment leading to the formation of a cohesive amorphous phase where internal cracking appeared severely limited. Such a notion might promote efficiency in industrial scale-up, as grinding could be limited for the obtainment of a coarser precursor that is still reactive, and a wider grain size range could be considered acceptable for use, saving on both grinding and sieving costs. Mortars obtained out of a PVG matrix yielded

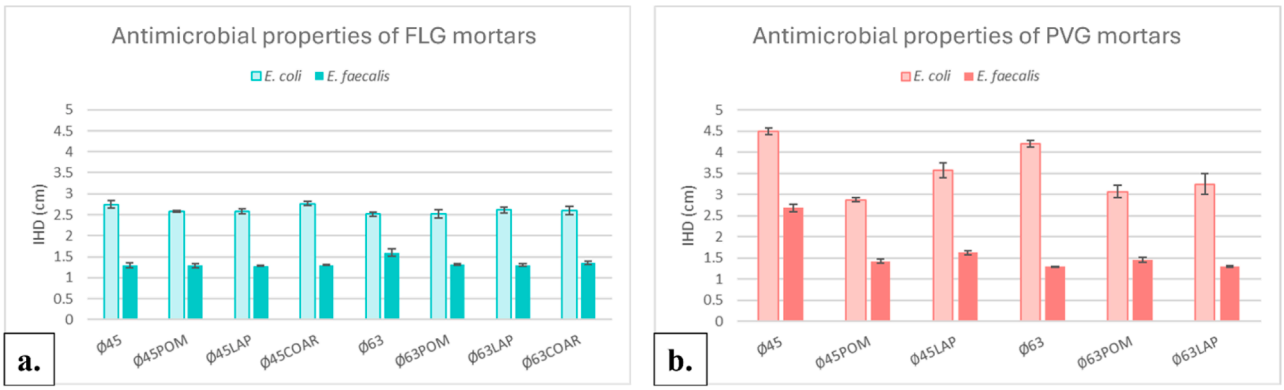

Fig. 17. Antimicrobial properties of FLG-based AAMs (a.) and PVG-based AAMs (b.). [REQUIRES COLOR IN PRINT].

more mixed results, with the interaction between the less reactive precursor and the fillers leading to generally higher compression strength compared to non-integrated pastes but also more substantial leaching of components. Overall, PVG-based formulations displayed less viable and reliable properties for use as construction material.

Leaching tests showed that the chemical attack of the glasses entailed by alkali activation broadly led to a higher susceptibility to leaching in AAMs compared to their precursors. The extent of release of certain pollutants, especially in FLG-based materials, render further optimization necessary for stabilization and environmentally viable application of the AAM formulations. A degree of antimicrobial activity was reported for all examined formulations and attributed to the high content and release of sodium, potassium and calcium highlighted by the leaching tests. In the case of PVG-based materials, markedly higher antimicrobial activity with respect to FLG-derived ones was attributed to the additional presence and activity of tellurium in the leaching environment. While this aspect of the PVG matrix may make it more suitable for inhibiting the growth of microbial colonies in surface and outdoor applications, the marginal enhancement in antimicrobial properties associated with leached metal ions could be constrained by material optimization aimed at limiting ion release. Moreover, this effect is ultimately outweighed by the comparatively inferior chemical and mechanical properties of activated panel glass relative to FLG.

Overall, experimental results were provided supporting the efficacy of mild activation as a methodology for recycling waste glass of complex composition, along with undesirable railings from extraction of volcanic rock, into low-emission, low-energy construction materials with desirable chemical and mechanical properties. Potential pathways towards strategy improvement were also highlighted, such as employment of the precursor in a wider granulometric range, and enhancement of internal ions stabilization via addition of more reactive precursor components and optimization of activation parameters.

Funding source

This work was performed in the context of the project “GLASS-based TREAtments for Sustainable Upcycling of inorganic RESidues (GLASS_Trea.S.U.Res)”, funded by the European Union – Next-GenerationEU - Piano Nazionale di Ripresa e Resilienza (PNRR) - Progetti di Ricerca di Rilevante Interesse Nazionale (PRIN) [#P2022S4TK2 CUP: E53D23017460001], Funding Decree D.D. 1385 of 01–09–2023. The public funding entity determined the topic of focus and established publication as an end goal for the experimental work, as dissemination was considered an express purpose of the project in its description.

CRediT authorship contribution statement

Emanuele De Rienzo: Writing – original draft, Methodology, Investigation, Data curation. **Francesco Carollo:** Writing – original draft, Methodology, Investigation, Data curation. **Antonio D’Angelo:** Writing – original draft, Methodology, Investigation, Data curation. **Luisa Barbieri:** Writing – review & editing, Supervision, Conceptualization. **Enrico Bernardo:** Writing – review & editing, Supervision, Resources, Funding acquisition, Conceptualization. **Michelina Catauro:** Writing – review & editing, Supervision, Funding acquisition, Conceptualization. **Cristina Leonelli:** Writing – review & editing, Validation, Supervision, Methodology, Conceptualization. **Isabella Lancellotti:** Writing – review & editing, Supervision, Funding acquisition, Conceptualization.

Declaration of competing interest

The authors declare that they have no known competing financial interests or personal relationships that could have appeared to influence the work reported in this paper.

References

[1] A. Magni Darwich Higuchi, M. Gorett Dos Santos Marques, L. Farias Ribas, R. Pereira De Vasconcelos, Use of glass powder residue as an eco-efficient supplementary cementitious material, Constr. Build. Mater. 304 (2021) 124640, https://doi.org/10.1016/j.conbuildmat.2021.124640.

[2] M.J. Zafar, H. Elsayed, E. Bernardo, Waste glass upcycling supported by Alkali activation: an overview, Materials (Basel) 17 (9) (2024) 2169, https://doi.org/10.3390/ma17092169.

[3] X. Wu, Z. Xiong, W. Zhu, X. Shan, E.H. Yang, Developing sustainable cement through Alkali-activation of waste glass and hydrophobic modification, Constr. Build. Mater. 479 (2025) 141507, https://doi.org/10.1016/j.conbuildmat.2025.141507.

[4] P. Su, S. Eniola, J. Xie, X. Zhao, C. Ugboaja, M. Li, R. Si, Q. Dai, Y. Fei, Y.H. Hu, Performance evaluation of glass powder as a partial precursor in Alkali-activated slag (AAS) binder and recycled glass and steel fibers in AAS mortar, Constr. Build. Mater. 473 (2025) 140757, https://doi.org/10.1016/j.conbuildmat.2025.140757.

[5] G. Tameni, D. Lago, H. Kaňková, L. Buňová, J. Kraxner, D. Galusek, D.M. Dawson, S. Ashbrook, E. Bernardo, Alkaline attack of boro-alumino-silicate glass: new insights of the molecular mechanism of cold consolidation and new applications, Open Ceram. 21 (2025) 100726, https://doi.org/10.1016/j.oceram.2024.100726.

[6] F. Carollo, E. De Rienzo, A. D’Angelo, P. Sgarbossa, L. Barbieri, C. Leonelli, I. Lancellotti, M. Catauro, E. Bernardo, Cold consolidation of waste glass by Alkali activation and curing by traditional and microwave heating, Materials (Basel) 18 (11) (2025) 2628, https://doi.org/10.3390/ma18112628.

[7] A.W. Ourgessa, J. Kraxner, H. Elsayed, D. Galusek, E. Bernardo, Sustainable construction materials from Alkali-activated waste fiberglass and waste refractory, Open Ceram. 20 (2024) 100678, https://doi.org/10.1016/j.oceram.2024.100678.

[8] M. Mahmoud, J. Kraxner, A. Mehta, H. Elsayed, D. Galusek, E. Bernardo, Alkali activation-induced cold consolidation of waste glass: application in organic-free direct ink writing of photocatalytic dye destructors, J. Eur. Ceram. Soc. 44 (9) (2024) 5449–5459, https://doi.org/10.1016/j.jeurceramsoc.2023.12.023.

[9] J.L. Provis, J.S.J. van Deventer, Introduction to geopolymers, in: J.L. Provis, J.S.J. van Deventer (Eds.), Geopolymers: Structure, processing, Properties and Industrial Applications, Woodhead Publishing Limited and CRC Press LLC, Boca Raton (FL), 2009, pp. 4–5.

[10] G. Dal Poggetto, M. Catauro, G. Crescente, C. Leonelli, Efficient addition of waste glass in MK-based geopolymers: microstructure, antibacterial and cytotoxicity investigation, Polymers (Basel) 13 (9) (2021) 1493, https://doi.org/10.3390/polym13091493.

[11] N. Shehata, E.T. Sayed, M.A. Abdelkareem, Recent progress in environmentally friendly geopolymers: a review, Sci. Total Environ. 762 (2021) 143166, https://doi.org/10.1016/j.scitotenv.2020.143166.

[12] L. Rossi, L. Miranda De Lima, Y. Sun, F. Dehn, J. Provis, G. Ye, G. De Schutter, Future perspectives for Alkali-activated materials: from existing standards to structural applications, RILEM Tech. Lett. 7 (2023) 159–177, https://doi.org/10.21809/rilemtechlett.2022.160.

[13] R. Navarro, E.G. Alcocel, I. Sánchez, M.A. Aguirre, E. Zornoza, Waste glass powder as silica source for the activator in the preparation of Alkali activated SiMn slag mortar, Constr. Build. Mater. 475 (2025) 141237, https://doi.org/10.1016/j.conbuildmat.2025.141237.

[14] M. Vidak Vasić, P. Muñoz Velasco, S. Bueno-Rodríguez, I. Netinger Grubeša, M. Dondi, L. Pérez Villarejo, D. Eliche-Quesada, C. Zanelli, State and perspectives of sustainable production of traditional silicate ceramics, Open Ceram. 17 (2024) 100537, https://doi.org/10.1016/j.oceram.2024.100537.

[15] A.W. Vieira, L.S. Rosso, A. Demarch, D. Pasini, S.P. Ruzza, S. Arcaro, M.J. Ribeiro, E. Angioletto, Life cycle assessment in the ceramic tile industry: a review, J. Mater. Res. Technol. 23 (2023) 3904–3915, https://doi.org/10.1016/j.jmrt.2023.02.023.

[16] D.D. Furszyfer Del Rio, B.K. Sovacool, A.M. Foley, S. Griffiths, M. Bazilian, J. Kim, D. Rooney, Decarbonizing the ceramics industry: a systematic and critical review of policy options, developments and sociotechnical systems, Renew. Sustain. Energy Rev. 157 (2022) 112081, https://doi.org/10.1016/j.rser.2022.112081.

[17] G. Tameni, E. Bernardo, Alkali activation of glass for sustainable upcycling: an overview, Ceramics 8 (2025) 108, https://doi.org/10.3390/ceramics8030108.

[18] E. Bernardo, H. Elsayed, A. Mazzi, G. Tameni, S. Gazzo, L. Contrafatto, Double-life sustainable construction materials from Alkali activation of volcanic ash/discarded glass mixture, Constr. Build. Mater. 359 (2022) 129540, https://doi.org/10.1016/j.conbuildmat.2022.129540.

[19] D. Lago, G. Tameni, J. Kraxner, D. Galusek, E. Bernardo, Cesium stabilization by engineered alkaline attack of glass for pharmaceutical containers, Mater. Lett. 372 (2024) 137097, https://doi.org/10.1016/j.matlet.2024.137097.

[20] U.N. Environment, K.L. Scrivener, V.M. John, E.M. Gartner, Eco-efficient cements: potential economically viable solutions for a low-CO_2 cement-based materials industry, Cem. Conc. Res. 114 (2018) 2–26, https://doi.org/10.1016/j.cemconres.2018.03.015.

[21] S. Ruan, G. Kastiukas, S. Liang, X. Zhou, Waste glass reuse in foamed Alkali-activated binders production: technical and environmental assessment, Front. Mater. 7 (2020) 581358, https://doi.org/10.3389/fmats.2020.581358.

[22] M. Torres-Carrasco, F. Puertas, Waste glass as a precursor in alkaline activation: chemical process and hydration products, Constr. Build. Mater. 139 (2017) 342–354, https://doi.org/10.1016/j.conbuildmat.2017.02.071.

[23] R. Seif, F.Z. Salem, N.K. Allam, E-waste recycled materials as efficient catalysts for renewable energy technologies and better environmental sustainability, Environ. Dev. Sustain. 26 (3) (2023) 5473–5508, https://doi.org/10.1007/s10668-023-02925-7.

[24] H.A. Ali, J.X. Lu, K. Sun, C.S. Poon, Valorization of spent fluorescent lamp waste glass powder as an activator for eco-efficient binder materials, Constr. Build. Mater. 352 (2022) 129020, https://doi.org/10.1016/j.conbuildmat.2022.129020.

[25] J.M. Esbrí, S. Rivera, J. Tejero, P.L. Higueras, Feasibility study of fluorescent lamp waste recycling by thermal desorption, Environ. Sci. Pollut. Res. 28 (43) (2021) 61860–61868, https://doi.org/10.1007/s11356-021-16800-3.

[26] R.A. Anwari, S. Coskun, M. Saltan, Research on recycle of waste fluorescent lamp glasses and use as mineral filler in asphalt mixture, J. Mater. Cycles Waste Manag. 25 (1) (2023) 258–271, https://doi.org/10.1007/s10163-022-01525-3.

[27] K. Treviño Rodríguez, A.I. Sánchez Vázquez, J.J. Ruiz Valdés, J. Ibarra Rodríguez, M.G. Paredes Figueroa, S. Porcar García, J.B. Carda Castelló, A. Álvarez Méndez, Photovoltaic glass waste recycling in the development of glass substrates for Photovoltaic applications, Materials (Basel) 16 (7) (2023) 2848, https://doi.org/10.3390/ma16072848.

[28] A. Surowiak, M. Wahman, Thermal–mechanical delamination for recovery of tempered glass from photovoltaic panels, Energies 17 (17) (2024) 4444, https://doi.org/10.3390/en17174444.

[29] K. Korniejenko, B. Kozub, A. Bąk, P. Balamurugan, M. Uthayakumar, G. Furtos, Tackling the circular economy challenges—Composites recycling: used tyres, wind turbine blades, and solar panels, J. Compos. Sci. 5 (9) (2021) 243, https://doi.org/10.3390/jcs5090243.

[30] K.Ekiz Barış, One-part Alkali-activated mortars based on clay brick waste, natural pozzolan waste, and marble powder waste, J. Sustain. Constr. Mater. Technol. 9 (4) (2024) 391–401, https://doi.org/10.47481/jscmt.1607828.

[31] F. Altimari, I. Lancellotti, C. Leonelli, F. Andreola, H. Elsayed, E. Bernardo, L. Barbieri, Green materials for construction industry from Italian volcanic quarry scraps, Mater. Lett. 333 (2023) 133615, https://doi.org/10.1016/j.matlet.2022.133615.

[32] R. Gutiérrez, M. Villaquirán-Caicedo, S. Ramírez-Benavides, M. Astudillo, D. Mejía, Evaluation of the antibacterial activity of a geopolymer mortar based on metakaolin supplemented with TiO_2 and CuO particles using glass waste as fine aggregate, Coatings 10 (2) (2020) 157, https://doi.org/10.3390/coatings10020157.

[33] M.C. Bignozzi, A. Saccani, L. Barbieri, I. Lancellotti, Glass waste as supplementary cementing materials: the effects of Glass chemical composition, Cem. Concr. Compos. 55 (2015) 45–52, https://doi.org/10.1016/j.cemconcomp.2014.07.020.

[34] L. Barbieri, F. Altimari, F. Andreola, B. Maggi, I. Lancellotti, Characterization of volcano-sedimentary rocks and related scraps for design of sustainable materials, Materials (Basel) 16 (9) (2023) 3408, https://doi.org/10.3390/ma16093408.

[35] C. Sgarlata, G. Dal Poggetto, F. Piccolo, M. Catauro, K. Traven, M. Češnovar, H. Nguyen, J. Yliniemi, L. Barbieri, V. Ducman, I. Lancellotti, C. Leonelli, Antibacterial properties and cytotoxicity of 100% waste derived Alkali activated materials: slags and stone wool-based binders, Front. Mater. 8 (2021) 689290, https://doi.org/10.3389/fmats.2021.689290.

[36] J. Kiventerä, P. Perumal, J. Yliniemi, M. Illikainen, Mine tailings as a raw material in Alkali activation: a review, Int. J. Miner. Metall. Mater. 27 (8) (2020) 1009–1020, https://doi.org/10.1007/s12613-020-2129-6.

[37] UNI EN 12457-2:2004, Characterisation of Waste - Leaching - Compliance Test for Leaching of Granular Waste Materials and Sludges - Part 2: One Stage Batch Test at a Liquid to Solid Ratio of 10 L/Kg for Materials with Particle Size Below 4 mm (Without or with Size Reduction), UNI, Rome, Italy, 2004.

[38] A. D'Angelo, V. Viola, M. Fiorentino, G. Dal Poggetto, I. Blanco, Use of natural dyes to color metakaolin-based geopolymer materials, Ceram. Int. 51 (5) (2025) 5528–5535, https://doi.org/10.1016/j.ceramint.2024.05.109.

[39] M. Mirzahosseini, K.A. Riding, Influence of different particle sizes on reactivity of finely ground glass as supplementary cementitious material (SCM), Cem. Concr. Compos. 56 (2015) 95–105, https://doi.org/10.1016/j.cemconcomp.2014.10.004.

[40] J. Lu, Z. Duan, C.S. Poon, Combined use of waste glass powder and cullet in architectural mortar, Cem. Concr. Compos. 82 (2017) 34–44, https://doi.org/10.1016/j.cemconcomp.2017.05.011.

[41] D.N. Varma, S.P. Singh, A review on waste glass-based geopolymer composites as a sustainable binder, Silicon 15 (18) (2023) 7685–7703, https://doi.org/10.1007/s12633-023-02629-7.

[42] L. Srinivasamurthy, V.S. Chevali, Z. Zhang, H. Wang, Phase changes under efflorescence in Alkali activated materials with mixed activators, Constr. Build. Mater. 283 (2021) 122678, https://doi.org/10.1016/j.conbuildmat.2021.122678.

[43] L.M. Henao Rios, A.F. Hoyos Trivino, M.A. Villaquiran-Caicedo, R. Mejía de Gutiérrez, Effect of the use of waste glass (as Precursor, and Alkali Activator) in the manufacture of geopolymer rendering mortars and architectural tiles, Constr. Build. Mater. 363 (2023) 129760, https://doi.org/10.1016/j.conbuildmat.2022.129760.

[44] G. Dal Poggetto, M. Catauro, G. Crescente, Cristina Leonelli, Efficient addition of waste glass in MK-based geopolymers: microstructure, antibacterial and cytotoxicity investigation, Polymers (Basel) 13 (9) (2021) 1493, https://doi.org/10.3390/polym13091493.

[45] M. Catauro, A. D'Angelo, S. Piccolella, C. Leonelli, Thermal influence on physico-chemical properties of geopolymers based on metakaolin and red tomato waste, Macromol. Symp. 404 (2022) 2100295, https://doi.org/10.1002/masy.202100295.

[46] A. Saccani, M.C. Bignozzi, L. Barbieri, I. Lancellotti, E. Bursi, Effect of the chemical composition of different types of recycled glass used as aggregates on the ASR performance of cement mortars, Constr. Build. Mater. 154 (2017) 804–809, https://doi.org/10.1016/j.conbuildmat.2017.08.011.

[47] L. Li, H. Zhang, X. Guo, X. Zhou, L. Lu, M. Chen, X. Cheng, Pore structure evolution and strength development of hardened cement paste with super low water-to-cement ratios, Constr. Build. Mater. 227 (2019) 117108, https://doi.org/10.1016/j.conbuildmat.2019.117108.

[48] M. Shaaban, W. Fouad Edris, A.A.K A. Al Sayed, R.S. Alrashidi, T.I. Selouma, Performance evaluation of alkaline activated geopolymer binders using RCA and industrial by-products as cement alternatives, Civ. Eng. J. 11 (2) (2025) 704–725, https://doi.org/10.28991/CEJ-2025-011-02-018.

[49] M.T. Bashir, M.J. Shinwari, R. Lal, M.A. Uddin, M.A. Sikandar, M.H. Rahman Sobuz, A. Almutairi, J. Wen, M.M. Hayet Khan, Experimental investigations of one-part geopolymer mortar: fresh, hardened, and durability properties using locally available industrial waste, Buildings 16 (2026) 37, https://doi.org/10.3390/buildings16010037.

[50] L.N. Assi, E. Deaver, M.K. ElBatanouny, P. Ziehl, Investigation of early compressive strength of fly ash-based geopolymer concrete, Constr. Build. Mater. 112 (2016) 807–815, https://doi.org/10.1016/j.conbuildmat.2016.03.008.

[51] M. Panizza, M. Natali, E. Garbin, V. Ducman, S. Tamburini, Optimization and mechanical-physical characterization of geopolymers with construction and demolition waste (CDW) aggregates for construction products, Constr. Build. Mater. 264 (2020) 120158, https://doi.org/10.1016/j.conbuildmat.2020.120158.

[52] N.I. Ahmad, Y.B. Kar, C. Doroody, T.S. Kiong, K.S. Rahman, M.N. Harif, N. Amin, A comprehensive review of flexible cadmium telluride solar cells with back surface field layer, Heliyon 9 (11) (2023) e21622, https://doi.org/10.1016/j.heliyon.2023.e21622.

[53] P. Duxson, J.L. Provis, G.C. Lukey, J.S.J. Van Deventer, F. Separovic, Z.H. Gan, ^{39}K NMR of free potassium in geopolymers, Ind. Eng. Chem. Res. 45 (26) (2006) 9208–9210, https://doi.org/10.1021/ie060838g.

[54] M.C. Kennedy, E.D. Ford, P. Singleton, M. Finney, J.K. Agee, Informed multi-objective decision-making in environmental management using Pareto optimality, J. Appl. Ecol. 45 (1) (2008) 181–192, https://doi.org/10.1111/j.1365-2664.2007.01367.x.

[55] X. Wei, F. Xie, C. Dong, P. Wang, J. Xu, F. Yan, Z. Zha, Safe disposal of hazardous waste incineration fly ash: stabilization/solidification of heavy metals and removal of soluble salts, J. Environ. Manage. 324 (2022) 116246, https://doi.org/10.1016/j.jenvman.2022.116246.

[56] X. Li, L. Yu, H. Zhou, G. Huang, C. Yang, F. Wu, Y. Zhang, An environment-friendly pretreatment process of municipal solid waste incineration fly ash to enhance the immobilization efficiency by Alkali-activated slag cement, J. Clean Prod. 290 (2021) 125728, https://doi.org/10.1016/j.jclepro.2020.125728.

[57] M. Ajorloo, M. Ghodrat, J. Scott, V. Strezov, Heavy metals removal/stabilization from municipal solid waste incineration fly ash: a review and recent trends, J. Mater. Cycles Waste Manag. 24 (2022) 1693–1717, https://doi.org/10.1007/s10163-022-01459-w.

[58] X. Yuan, X. Zhao, Y. Chen, Z. Yang, J. Yang, Stabilization effect of chelating agents on heavy metals in two types of municipal solid waste incineration fly ash, Process Saf. Environ. Prot. 180 (2023) 169–180, https://doi.org/10.1016/j.psep.2023.09.068.

[59] F. Genua, M. Giovini, C. Leonelli, I. Lancellotti, Chelating, reducing, and adsorbing agents in geopolymers for heavy metals stabilization from galvanic sludge, Polymers (Basel) 18 (1) (2026) 28, https://doi.org/10.3390/polym18010028.

[60] A. Tesovnik, L.M. Ottosen, V. Ducman, Carbonation of lightweight alkali-activated aggregates based on biomass fly ash: effect on microstructure and leaching behavior, Case Stud. Const. Mater. 23 (2025) e05014, https://doi.org/10.1016/j.cscm.2025.e05014.

[61] S.O. Hagge, M.U. Hammer, A. Wiese, U. Seydel, T. Gutsmann, Calcium adsorption and displacement: characterization of lipid monolayers and their interaction with membrane-active peptides/proteins, BMC Biochem. 7 (1) (2006) 15, https://doi.org/10.1186/1471-2091-7-15.

[62] M.A. Swairjo, N.O. Concha, M.A. Kaetzel, J.R. Dedman, B.A. Seaton, Ca^{2+}-bridging mechanism and phospholipid head group recognition in the membrane-binding protein annexin V, Nat. Struct. Mol. Biol. 2 (11) (1995) 968–974, https://doi.org/10.1038/nsb1195-968.

[63] L. Peng, R. Lifang, X. Hongyu, L. Xi, Z. Chaocan, Study on the toxic effect of lead(II) ion on *Escherichia coli*, Biol. Trace Elem. Res. 115 (2007) 195–202, https://doi.org/10.1007/BF02686030.

[64] J. Stautz, Y. Hellmich, M.F. Fuss, J.M. Silberberg, J.R. Devlin, R.B. Stockbridge, I. Hänelt, Molecular mechanisms for bacterial potassium homeostasis, J. Mol. Biol. 433 (16) (2021) 166968, https://doi.org/10.1016/j.jmb.2021.166968.

[65] P. Kumar, T. Kumar, S. Singh, N. Tuteja, R. Prasad, J. Singh, Potassium: a key modulator for cell homeostasis, J. Biotechnol. 324 (2020) 198–210, https://doi.org/10.1016/j.jbiotec.2020.10.018.

[66] K. Nakajo, R. Komori, S. Ishikawa, T. Ueno, Y. Suzuki, Y. Iwami, N. Takahashi, Resistance to acidic and alkaline environments of endodontic pathogen Enterococcus Faecalis, Oral. Microbiol. Immunol. 21 (2006) 283–288, https://doi.org/10.1111/j.1399-302X.2006.00289.

[67] P.H. Weckwerth, R.O. Zapata, R.R. Vivan, M. Tanomaru Filho, A.G.A. Maliza, M.A. H. Duarte, In vitro alkaline pH resistance of Enterococcus Faecalis, Braz. Dent. J. 24 (5) (2013) 474–476, https://doi.org/10.1590/0103-6440201301731.

[68] L. Zhang, L. Ye, Z. Yin, K. Xiao, C. Jing, Mechanistic study of antimonate reduction by *Escherichia coli* W3110, Environ. Poll. 291 (2021) 118258, https://doi.org/10.1016/j.envpol.2021.118258.

[69] A. Tang, Q. Ren, Y. Wu, C. Wu, Y. Cheng, Investigation into the antibacterial mechanism of biogenic tellurium nanoparticles and precursor tellurite, Int. J. Mol. Sci. 23 (19) (2022) 11697, https://doi.org/10.3390/ijms231911697.